Complementary substrate specificity and distinct quaternary assembly of the Escherichia coli aerobic and anaerobic beta-oxidation trifunctional enzyme complexes

Sah-Teli, Shiv K.

2019-07-15

Sah-Teli , S K , Hynönen , M J , Schmitz , W , Geraets , J A , Seitsonen , J , Pedersen , J S , Butcher , S J , Wierenga , R K & Venkatesan , R 2019 , ' Complementary substrate specificity and distinct quaternary assembly of the Escherichia coli aerobic and anaerobic beta-oxidation trifunctional enzyme complexes ' , Biochemical Journal , vol. 476 , pp. 1975-1994 . https://doi.org/10.1042/BCJ20190314

http://hdl.handle.net/10138/317733
https://doi.org/10.1042/BCJ20190314

unspecified
acceptedVersion

Complementary substrate specificity and distinct quaternary assembly of the *Escherichia coli* aerobic and anaerobic beta-oxidation trifunctional enzyme complexes

Shiv K. Sah-Teli[1], Mikko J. Hynönen[1], Werner Schmitz[2], James A. Geraets[3,4], Jani Seitsonen[3], Jan Skov Pedersen[5], Sarah J. Butcher[3], Rik K. Wierenga[1] and Rajaram Venkatesan[1*]

[1]Faculty of Biochemistry and Molecular Medicine, and Biocenter Oulu, University of Oulu, Finland

[2]Theodor-Boveri-Institut für Biowissenschaften der Universität Würzburg, Germany

[3]Helsinki Institute of Life Science, University of Helsinki, Finland

[4]Forschungszentrum Jülich, Jülich, Germany

[5]Department of Chemistry and Interdisciplinary Nanoscience Center (iNANO), Aarhus University, Denmark

*rajaram.venkatesan@oulu.fi

Running Title

Structural enzymological studies of the *E. coli* trifunctional enzyme (TFE) complexes

Abstract

The trifunctional enzyme (TFE) catalyzes the last three steps of the fatty acid β-oxidation cycle. Two TFEs are present in *Escherichia coli*, EcTFE and anEcTFE. EcTFE is expressed only under aerobic conditions whereas anEcTFE is expressed also under anaerobic conditions, with nitrate or fumarate as the ultimate electron acceptor. The anEcTFE subunits have higher sequence identity with the human mitochondrial TFE (HsTFE) than with the soluble EcTFE. Like HsTFE, here it is found that anEcTFE is a membrane bound complex. Systematic enzyme kinetic studies show that anEcTFE has preference for medium and long chain enoyl-CoAs, similar to HsTFE, whereas EcTFE prefers short chain enoyl-CoA substrates. The biophysical characterization of anEcTFE and EcTFE shows that EcTFE is heterotetrameric, whereas anEcTFE is purified as a complex of two heterotetrameric units, like HsTFE. The tetrameric assembly of anEcTFE resembles the HsTFE tetramer, although the arrangement of the two anEcTFE tetramers in the octamer is different from the HsTFE octamer. These studies demonstrate that EcTFE and anEcTFE have complementary substrate specificities, allowing for complete degradation of long chain enoyl-CoAs under aerobic conditions. The new data agree with the notion that anEcTFE and HsTFE are evolutionary closely related, whereas EcTFE belongs to a separate subfamily.

Keywords

Fatty acid oxidation, trifunctional enzyme, enzymology, small-angle scattering, electron microscopy

Abbreviations list

ACP: acyl carrier protein

AD: acyl Coenzyme A dehydrogenase

anEcTFE: anaerobic *E. coli* TFE

BN-PAGE: blue native polyacrylamide gel electrophoresis

BSA: bovine serum albumin

$C_{12}E_{9:}$ polyoxyethylene (9) dodecyl ether

CD: circular dichroism

CHAPS: 3-[(3-cholamidopropyl)-dimethylammonio]-1-propanesulfonate

CoA: coenzyme A

CYMAL-6: 6-cyclohexylhexyl β-D-maltoside

DDM: dodecyl-β-D-maltoside

DLS: dynamic light scattering

DMNG: decyl maltose neopentyl glycol

ECH: enoyl coenzyme A hydratase

EcTFE: aerobic *E. coli* TFE

EM: electron microscopy

HAD: 3S-hydroxyacyl-CoA dehydrogenase

HEPES: 4-(2-hydroxyethyl)-1-piperazineethanesulfonic acid

HsTFE: Human mitochondrial TFE

IMAC: immobilized metal affinity chromatography

IPTG: isopropyl β-D-1-thiogalactopyranoside

KAT: 3-ketoacyl-CoA thiolase

LDAO: lauryldimethylamine-N-Oxide

MCS: multiple cloning site

MFE-1: multifunctional enzyme (type-1)

MtTFE: *Mycobacterium tuberculosis* TFE

Ni^{2+}-NTA: Ni^{2+}-nitrilotriacetate

β-OG: octyl-β-glucoside

PfTFE: *Pseudomonas fragi* TFE

PHA: polyhydroxy alkanoate

SAXS: small angle X-ray scattering

SDS-PAGE: sodium dodecyl sulphate polyacrylamide gel electrophoresis

SEC: size exclusion chromatography

SLS: static light scattering

TCA: tricarboxylic acid cycle

TFE: trifunctional enzyme

24E,25DM-THCeA: *24E*, *25*-demethylated-trihydroxycholestenoyl-CoA

24E-THCeA: *24E*-trihydroxycholestenoyl-CoA

T_m: melting temperature

Tris: tri(hydroxymethyl)aminomethane

VLCAD: very-long-chain AD

Introduction

Fatty acids and their derivatives play a central role in many cellular processes. They act as a major source of energy and carbon and are metabolized in several degradative and biosynthetic pathways. The fatty acids are conjugated via a thioester bond to the pantetheine moiety of either CoA (in the degradative β-oxidation pathway) or of ACP (in biosynthetic pathways). In the mitochondrial and bacterial β-oxidation pathways the fatty acid moiety of acyl-CoA is shortened by the repeated removal of two carbon units in four steps by the enzymes AD (EC:1.3.8.7), ECH (EC:4.2.1.17), HAD (EC: 1.1.1.35) and KAT (EC: 2.3.1.16) respectively.

In *Escherichia coli* the AD reaction is catalyzed by the enzyme *fadE* [1], whereas the remaining three reactions are catalyzed by the soluble TFE complex (EcTFE), made from two polypeptide chains that are encoded by the genes *fadB* and *fadA*. *fadB* encodes the α-subunit of TFE with ECH and HAD activities, whereas *fadA* encodes the β-subunit of TFE which is a thiolase [2,3]. No recombinant protein expression studies have been reported so far for EcTFE although enzyme kinetic studies have been carried out with the endogenously expressed EcTFE [4].

In 2002, a second *E. coli* β-oxidation TFE complex, whose α- and β-subunits are encoded by the genes *fadJ* (also known as *yfcX*) and *fadI* (also known as *yfcY*), respectively, was identified [1,5]. Snell and coworkers have shown that *fadJ* has ECH and HAD activities whereas *fadI* catalyzes the thiolase reaction using the recombinantly expressed and purified *fadJ* and *fadI*. Cronan and coworkers demonstrated that the *fadI/fadJ*-TFE functions under anaerobic conditions, when nitrate is present as an electron acceptor [1], and therefore this TFE is referred to as the anEcTFE. The previously discovered EcTFE is a soluble enzyme and it functions under aerobic conditions. More recently, genetic complementation studies showed that the protein encoded by *ydiO* is the acyl-CoA dehydrogenase that functions in the anaerobic β-oxidation pathway [6] (Figure 1), having therefore the same role as *fadE* in the aerobic β-oxidation pathway. These researchers also showed that other auxiliary proteins (of the QRST gene) are required for a functional anaerobic respiratory electron transport system.

In spite of the long history of the study of the *E. coli* β-oxidation enzymes, molecular level studies of these enzymes including detailed enzymatic and structural characterizations are very limited. In particular, there are very few reports describing the properties of anEcTFE. Snell and coworkers have shown that anEcTFE-α activity is essential for the *E. coli fadB* mutant strain to produce medium chain length PHAs when fed with hexadecanoic (palmitic) or decanoic acids indicating that anEcTFE is involved also in the aerobic chain shortening process. When both *fadB* and *fadJ* are disrupted, the

chain length of the PHAs could not be reduced compared to the length of the carbon chain fed in the medium [7]. Studies from Olivera and coworkers revealed the presence of two distinct β-oxidation pathways also in *Pseudomonas putida* [8], and the respective *fadI* and *fadJ* genes are also found in the genomes of several pathogenic bacteria such as Shigella and Salmonella as well as of pathogenic *E. coli* strains, which are all believed to encounter anaerobic growth conditions during their life cycle [1]. Recent studies have also reported the importance of anaerobic respiration using nitrate and/or fumarate as an electron acceptor for the successful enterohemorrhagic *E. coli* colonization of the streptomycin treated mouse intestine [9,10].

In mammals, the β-oxidation happens in peroxisomes and mitochondria. Mitochondria have membrane associated VLCAD [11] and TFE [12] (proposed to be bound to only the inner leaflet of the mitochondrial membrane), which carry out the first and the next three steps of the β-oxidation cycle, respectively (Figure 1) for very-long-chain acyl-CoA molecules. In addition to VLCAD and TFE, there are also soluble monofunctional mitochondrial enzymes which catalyze the β-oxidation of short and medium chain fatty acyl-CoAs. The first crystal structure of a soluble TFE to be determined was the *Pseudomons fragi* TFE (PfTFE) [13], which is a close homolog of EcTFE sharing a sequence identity of 56% and 63% for the α- and β-subunits, respectively. The structure of the soluble TFE from *Mycobacterium tuberculosis* (MtTFE) [14] showed that, in spite of the similar tertiary structure of the individual subunits, MtTFE forms a strikingly different quaternary structure when compared to PfTFE. This was attributed to the presence of a unique 25 amino acid insertion in the thiolase subunit of MtTFE. Unlike *E. coli*, *M. tuberculosis* has only one TFE although this species has many monofunctional β-oxidation enzymes. A phylogenetic sequence analysis of TFEs from various organisms suggests that there are at least four TFE subfamilies namely, bacterial aerobic TFE, bacterial anaerobic TFE, mycobacterial TFE and mitochondrial TFE [14]. The assembly and crystal structures of bacterial aerobic and mycobacterial TFEs are now known. During the preparation of this manuscript, the cryoEM and crystal structures of HsTFE were reported [15,16]. HsTFE forms a third type of quaternary assembly in good agreement with the proposal of four TFE-subfamilies [14]. However, the assembly of the bacterial anaerobic TFE is not known. The phylogenetic sequence analyses suggest that anEcTFE is most closely related to HsTFE [14,17].

The presence of substrate channeling in fatty acid metabolism has been reported from *in vivo* studies [18,19] as well as from *in vitro* studies, for example for EcTFE [4] and mitochondrial (porcine) TFE [20]. Recent experimental studies on lipid metabolizing enzyme systems have suggested two mechanisms how substrate channeling can be achieved, being by sharing a common anchoring site for the intermediate [21] or by generating a catalytic cavity [22]. Based on the structure of PfTFE a

possible substrate channeling mechanism for PfTFE has been proposed. According to this proposal, ECH and HAD share the same binding pocket for the adenine base of *2E*-hexadecenoyl-CoA in PfTFE while the long acyl group travels between the ECH and HAD catalytic sites [13,23]. From the HsTFE crystal structure a somewhat similar substrate channeling mechanism is inferred, but in addition this analysis suggests that the cavity between the TFE active sites and the membrane to which this TFE is anchored could also play an important role [16], As the assemblies of the three known TFEs from three different TFE-subfamilies are different, the mechanism of substrate channeling between the two subunits are expected to be different. In the crowded intracellular milieu [24], substrate channeling has several advantages like avoiding multiple solvation/desolvation steps, avoiding accumulation of inhibitory and/or reactive intermediates, facilitating reactions to proceed despite a highly unfavorable equilibrium [25] and making efficient use of the available mitochondrial CoA pool [20]. This property appears to be important also in biotechnological applications of enzymes [22,26]. In order to study the substrate channeling mechanism in these TFEs, it is essential to systematically characterize their structural and kinetic properties. In this study the kinetic and structural properties of the recombinantly expressed and purified EcTFE and anEcTFE complexes are reported. The kinetic properties are also compared with the kinetic properties of HsTFE to better understand the evolutionary relation between these TFEs. These structural and kinetic studies provide new insight into the assembly and substrate specificity properties of EcTFE and anEcTFE, which is essential for further understanding of their molecular properties.

Materials and Methods

Cloning and overexpression

The *E. coli* K12 MG1655 genes *fadB* (EcTFE-α, UniProtKB: P21177) and *fadA* (EcTFE-β, UniProtKB: P21151) were cloned into the MCS 1 of pETDuet-1 and MCS2 of the pACYC-Duet-1 expression vector, respectively, using the restriction free PCR approach with appropriate primers (Supplementary Table 1). Similarly, the *fadJ* (anEcTFE-α, UniProtKB: P77399) and *fadI* (anEcTFE-β, UniProtKB: P76503) were cloned into MCS1 and MCS2 of pETDuet-1 resulting in the anEcTFE (His-α/β) construct. The anEcTFE (α/His-β) construct was also cloned in the pETDuet-1 vector using the same approach. The genes *HADHA* (HsTFE-α, UniProtKB: P40939) and *HADHB* (HsTFE-β, UniProtKB: P55084) were amplified by PCR using the *HADHA*-cDNA and codon optimized *HADHB*-cDNA (GenScript, Piscataway, USA) as the template, respectively and cloned in MCS1 and MCS2 of pRSFDuet-1 vector resulting in the HsTFE (α/His-β) in a similar manner. The gene sequences in the final constructs were verified by DNA sequencing. The EcTFE, anEcTFE and

HsTFE constructs were transformed into *E. coli* BL21DE3, BL21DE3pLys and Rosetta DE3 pLys strains, respectively and cultured in M9ZB media with suitable antibiotics at 37 ºC. Expression of TFE was induced with 0.2 mM IPTG at 0.6 OD overnight at 22 ºC.

Purification

EcTFE

Cells expressing EcTFE were harvested and resuspended in the lysis buffer (50 mM Tris, 0.5 M NaCl, 10% glycerol, 5 mM imidazole, pH 8.0). After lysis, the cell debris were removed by centrifugation at 30000g for 45 minutes and EcTFE was purified from the soluble fraction by Ni^{2+}-NTA affinity chromatography. The eluted fractions were concentrated and loaded on a Superdex 200 Hiload 16/60 column (GE Healthcare, Chicago, Illinois, USA) pre-equilibrated with 20 mM HEPES containing, 120 mM KCl, 2.5 mM DTT, pH 7.2. Pure EcTFE fractions were concentrated to 10 mg mL^{-1} and stored at -70 ºC for further studies. The yield is about 5 mg of EcTFE per 1 L culture.

anEcTFE

The anEcTFE expressing cells were resuspended in lysis buffer (20 mM Tris, 500 mM NaCl, 10% glycerol, 5 mM imidazole, pH 8.0). After cell lysis and removing the cell debris, the membrane fraction was isolated from the supernatant by ultracentrifugation at 370000g for 1 hour at 4 °C. anEcTFE was solubilized from the membrane fraction by overnight incubation with the extraction buffer (lysis buffer containing one of the detergents, which are 0.5% w/v LDAO, 0.5% w/v DDM, 0.5% v/v $C_{12}E_9$, 1% w/v β-OG, 0.5% v/v CYMAL-6, 0.1% w/v DMNG or 1% w/v CHAPS (Anatrace, Maumee, Ohio, USA)) at 4 °C. Solubilized anEcTFE was purified from the supernatant by Co^{2+}-Talon affinity purification. The eluted anEcTFE was concentrated and loaded to a Superdex 200 HiLoad 16/60 (GE Healthcare, Chicago, Illinois, USA) column, pre-equilibrated with 50 mM Tris buffer, 0.5 M NaCl, 5% glycerol, 2.5 mM DTT pH 8.0 containing 0.05% (v/v) $C_{12}E_9$ or 0.15% w/v LDAO or 0.15% w/v DDM or 0.5% w/v β-OG or 0.15% v/v CYMAL-6 or 0.1% w/v DMNG or 0.5% w/v CHAPS (Figure 2c). Pure anEcTFE fractions were concentrated and stored at -70 ºC for further studies. Approximately 0.5 mg of anEcTFE is obtained per 1 L of culture.

HsTFE

The HsTFE expressing cells were resuspended in lysis buffer (20mM Tris, 500 mM NaCl, 5 mM imidazole, 0.1% $C_{12}E_9$ or (0.15% w/v LDAO or 0.15% w/v DDM or 0.5% w/v β-OG or 0.15% v/v CYMAL-6 or 0.1% w/v DMNG or 0.5% w/v CHAPS (Anatrace, Maumee, Ohio, USA)) pH 8.0.

After lysis, the cell debris were removed by centrifugation at 30000g for 45 minutes and HsTFE was purified from the soluble fraction by affinity chromatography using Co^{2+}-Talon beads. The eluted HsTFE was concentrated and loaded on to Superdex 200 Hiload 16/60 column (GE Healthcare, Chicago, Illinois, USA) pre-equilibrated with 50 mM Tris, 500 mM NaCl, 2.5 mM DTT and 0.05% $C_{12}E_9$ or (0.15% w/v LDAO or 0.15% w/v DDM or 0.5% w/v β-OG or 0.15% v/v CYMAL-6 or 0.1% w/v DMNG or 0.5% w/v CHAPS) pH 8.0 (Figure 2d). The pure HsTFE fractions from SEC were concentrated and stored at -70 ºC. About 0.5 mg of HsTFE can be purified from 1 L culture.

CD spectroscopy

The protein (EcTFE: 0.1 mg mL^{-1}; anEcTFE: 0.05 mg mL^{-1}; HsTFE: 0.05 mg mL^{-1}) was exchanged into 10 mM potassium phosphate buffer at pH 7.6 for the CD measurements (Chirascan CD spectrophotometer, Applied Photophysics, Surrey, UK). For the determination of the T_m, the sample was heated at a rate of 1 °C per min from 22 to 94 °C. The melting curves were calculated by comparing the spectra from 190-280 nm with the global fit analysis protocol as implemented in the Global3 software.

DLS and SLS

The polydispersity of the purified proteins was measured using the Wyatt dynamic light scattering plate reader-II at a concentration of 0.1 mg mL^{-1} at 22 ºC in duplicates. SLS measurements were made by injecting 500 µg of the protein onto a Superdex 200 10/300 GL column (GE Healthcare, Chicago, Illinois, USA) connected to an Äkta purifier protein purification system, a Shodex refractive index detector and a Wyatt SLS detector. The molecular mass of the protein in the eluted peak was calculated by the ASTRA software.

BN-PAGE

About 50 µg of protein mixed with sample buffer (0.1% Coomassie G-250 added into 4x native sample buffer) without SDS and β-mercaptoethanol was loaded in the wells of 4-13% gradient native gels and run for 2-3 hours at 80 volt [27].

Synthesis of the unsaturated enoyl-CoA derivatives

Acetoacetyl-CoA and *2E*-butenoyl-CoA were purchased from Sigma-Aldrich (Missouri, USA). *2E*-decenoic acid and other chemicals used for substrate synthesis were from Merck (Darmstadt, Germany). 2-methyl-*2E*-decenoic acid, *2E*-hexadecenoic acid, *24E*-THCeA and *24E*,25DM-THCeA were synthesized by the Wittig reaction using carbomethoxymethylene- or

ethoxycarbonylethylidene-triphenylphosphoranes and aldehydes (octanal, tetradecanal and cholic acid aldehyde), which were obtained by the reduction of the corresponding acids. Pristenoic acid was synthesized from phytol as described previously [28]. *2E,4E*-decadienoic acid was synthesized by the Pinnick oxidation of *2E,4E*-decadienol [29]. Activation of carboxylic acids to their corresponding CoA esters was done by the mixed anhydride method [28]. The identity of the acyl-CoA esters was confirmed by TLC-, [^{1}H] NMR- and HR-MS-analysis.

Enzyme activity measurements

The enzyme activity measurements of the ECH, the HAD and the thiolase reactions were performed at 25 ºC using the Jasco V660 spectrophotometer and monitored for 180 s [14]. The initial rates were obtained using the linear parts of the progress curves. For the ECH and the HAD activities, progress curves were recorded at different substrate concentrations and subsequently the k_{cat} and K_m values were determined from the Michaelis-Menten plots for the ECH and HAD activities of EcTFE, anEcTFE and HsTFE with *2E*-butenoyl-CoA, *2E*-decenoyl-CoA and *2E*-hexadecenoyl-CoA. The precise assay conditions are listed below and the k_{cat} and K_m values obtained under these conditions are referred to as the apparent Michaelis-Menten constants. In addition, specific enzyme activities for a number of other substrates (Figure 3) were determined at a substrate concentration of 60 µM.

ECH activity

The ECH activity was measured in a direct assay at 263 nm (at 300 nm for *2E,4E*-decadienoyl-CoA) to monitor the disappearance of the C-C double bond of the *2E*-enoyl-CoA substrate. The reaction mixture (500 µL) contained 0.5 µM to 120 µM of the substrate in 50 mM Tris buffer containing 50 mM KCl and 50 µg mL^{-1} BSA at pH 9.0. The ECH reaction was initiated by adding 48 ng EcTFE or 60 ng anEcTFE/ HsTFE to the reaction mixture. The molar extinction coefficient of 6700 M^{-1} cm^{-1} (25400 M^{-1} cm^{-1} for *2E,4E*-decadienoyl-CoA) was used for calculating the specific activities.

HAD activity

The HAD activity was measured at 340 nm to monitor the formation of NADH. The 3S-hydroxyacyl-CoA substrate of the HAD active site is generated by the hydratase active site from the enoyl-CoA substrate and its concentration is used when analyzing the kinetic data. The reaction mixture (500 µL) contained 0.5 µM to 120 µM enoyl-CoA substrate, 1 mM NAD^+ and 1 mM CoA in 50 mM Tris buffer with 50 mM KCl, 50 µg mL^{-1} BSA at pH 9.0. The HAD reaction was started by adding 120 ng EcTFE or 240 ng anEcTFE / HsTFE to the reaction mixture. The molar extinction coefficient of 6200 M^{-1} cm^{-1} was used for calculating the specific activities.

KAT activity

The KAT activity was measured at 303 nm to monitor the disappearance of the Mg^{2+}-3-ketoacyl-CoA complex. The reaction mixture (500 µL) contained 1 mM NAD^+, 5 mM $MgCl_2$ and 0.5 mM CoA in 50 mM Tris buffer at pH 8.5 with 50 mM KCl, 50 µg mL^{-1} BSA. The reaction was started by adding 240 ng of EcTFE, anEcTFE, or HsTFE to the reaction mixture and the reaction was monitored for 180 s. The short chain acetoacetyl-CoA substrate (60 µM) was directly added to the assay buffer. The medium and long chain 3-ketoacyl-CoA compounds (3-ketodecanoyl-CoA and 3-ketohexadecanoyl-CoA) were generated by incubating 60 µM of the corresponding *2E*-enoyl-CoAs with 240 ng of EcTFE or anEcTFE or HsTFE for 5-10 minutes in the enzyme assay buffer (50 mM Tris buffer at pH 8.5 with 50 mM KCl, 50 µg mL^{-1} BSA) with 1 mM NAD^+ and 5 mM $MgCl_2$. The appearance of the Mg^{2+}-3-ketoacyl-CoA complex was monitored at 303 nm until a plateau was reached. The thiolase reaction was then initiated by adding 0.5 mM CoA to the incubation mixture and the breakdown of the Mg^{2+}-3-ketoacyl-CoA complex was monitored at 303 nm. The molar extinction coefficient of 21400 M^{-1} cm^{-1} for the Mg^{2+}-acetoacetyl-CoA complex and 13900 M^{-1} cm^{-1} for the longer chain Mg^{2+}-3-ketoacyl-CoA complexes was used for calculating the specific activities.

SAXS

SAXS experiments for EcTFE and anEcTFE were carried out at beamline B21, Diamond Light Source, UK, and BM29-BIOSAXS beamline at ESRF, France, respectively, in HPLC mode. 30 µL of EcTFE (6.2 mg mL^{-1}) and the Shodex KW-403 column pre-equilibrated with 20 mM HEPES, 120 mM KCl, 2.5 mM DTT, pH 7.2 were used. Scattered X-rays at a wavelength of 1 Å (at 12.4 keV) were recorded with a Pilatus 2M detector. A freshly prepared BSA solution at 4.4 mg mL^{-1} was used for calibrating the molecular mass. Similarly, SAXS data from anEcTFE (30 µL at 3.5 mg mL^{-1}) passed through a Superdex 200 5/150 GL column (GE Healthcare, Chicago, Illinois, USA) pre-equilibrated with 50 mM Tris, 500 mM NaCl, 5% glycerol, 0.05% $C_{12}E_9$, 2.5 mM DTT at pH 8.0 were recorded on a Pilatus 1M detector at a wavelength of 1 Å (at 12.5 keV). The freshly prepared BSA solution at 4.75 mg mL^{-1} was used for calibrating the molecular mass. More detailed data collection parameters are listed in Supplementary Table 2. Additionally, a few measurements were performed at the home-lab SAXS instrument at Aarhus University, Denmark [30]. anEcTFE samples with excess of $C_{12}E_9$ as well as samples with only $C_{12}E_9$ including also some with concentrations above the critical micelle concentration of the detergent were also measured.

The buffer averaged scattering was subtracted from the protein X-ray scattering for all the samples and further analysis was carried out using the program SCATTER [31] and PRIMUS [32]. The radius

of gyration R_g, forward scattering I_0, the maximum dimensions D_{max} and the interatomic distance distribution functions *P(r)* were estimated using the Guinier approximation of the GNOM package [33] in SCATTER and PRIMUS. The molecular mass of the protein in solution was estimated using protein volume from the Porod invariant (MM_{qp}), SAXMoW tool (MoW), empirical volume of correlation (V_c) and Size&Shape methods implemented in DATTOOLS from ATSAS package as described recently [34]. The output from GNOM was further used to generate the *ab initio* shapes using DAMMIN of the online-SAXS cluster at EMBL, Hamburg [35,36] and for calculating low resolution electron density maps using the DENSSWeb server with the default parameters [37]. The built atomic models were compared against the experimental SAXS data using FoXS [38], CRYSOL [39] and WLSQ_PDBX [40], which also allows inclusion of the scattering from $C_{12}E_9$ micelles as an extra component to enable description of samples that may have coexisting micelles. The reduced χ^2 values were calculated and used for assessing the quality of the fits. All the structures were visualized with PyMOL (The PyMOL Molecular Graphics System, Version 2.0 Schrödinger, LLC.) and the density maps were visualized with chimera (UCSF, chimera2) [41].

Modeling of the tetrameric TFE assemblies

First, the structural models of the individual subunits of EcTFE and anEcTFE were obtained using the corresponding subunits of PfTFE (PDB code: 1WDM) and HsTFE (PDB code: 5ZQZ), respectively, based on the target-template alignment using ProMod3 by the SWISS-MODEL server [42]. The heterotetrameric EcTFE (Figure 4) and anEcTFE assemblies were then generated using the PfTFE and HsTFE structures respectively as the reference. The HsTFE octameric assembly (PDB code: 5ZRV) was used to generate the initial model of the anEcTFE octameric assembly (Figure 5). The SSM superpose option [43] in COOT [44] was used for all superposition calculations. The secondary structure contents of both heterotetrameric EcTFE and heterooctameric anEcTFE models were analyzed by the STRIDE web interface [45].

Negative staining EM studies

EcTFE was treated with 0.01% glutaraldehyde and incubated in ice for 1 hour for crosslinking. The reaction was stopped by adding 10% 1 M Tris pH 8.0 and further passed through a SEC column. 3 µL of the peak fraction (0.025 mg mL^{-1}) was applied to the quantifoil standard holey carbon grid, stained with 1% uranyl acetate and 83 images were collected manually from homogeneously stained regions under Tecnai G2 spirit TEM at 100 kV with 1.4 s exposure time at 49k magnification (at Biocenter Oulu EM core facility, Oulu). 3 µL of anEcTFE (0.025 mg mL^{-1}) was applied to the quantifoil standard holey carbon grid, stained with 1% potassium phosphotungstate pH 7.0 and 60

images were collected manually under FEI Tecnai F20 TEM at 200 kV with 1 s exposure at 82K magnification (at Biocenter Finland EM facility, Helsinki). All the images (.mrc format) from both samples were initially processed by the emanbox program of EMAN2 [46]. In brief, 74,000 EcTFE particles were picked and processed for 2D classification in RELION [47]. 23,000 particles were then selected and processed for 3D classification using a reference 3D map generated from the PfTFE (PDB code: 1WDK) structure with 60 Å low pass filter. Finally, the 3D map of EcTFE was generated at 24 Å resolution from 7,000 particles in 3D autorefine run using a reference map and mask generated from one of the previously generated 3D classes. Similarly, 31,000 anEcTFE particles were picked and processed for 2D classification and 6,600 particles were then selected and processed for 3D classification using a reference 3D map generated with the EMAN2 program using particles from a subset of images. Finally, the 3D map of anEcTFE was generated at 23 Å resolution from 4,200 particles in 3D autorefine run using a reference map and mask generated from one of the previously generated 3D classes. Both the EcTFE and anEcTFE final 3D maps were visualized and the atomic models were fitted in the corresponding map using the fit-into-map tool of chimera (UCSF, chimera2) [41].

Results

Oligomeric state of EcTFE

The genes encoding EcTFE-α and EcTFE-β were cloned in such a way, that only EcTFE-α was expressed with an N-terminal His_6-tag. Upon coexpression, EcTFE-β copurified with EcTFE-α during the Ni^{2+}-NTA affinity purification and the complex eluted as a single peak in the subsequent SEC experiment (Figure 2a and Supplementary Figure 3a). The molecular mass of the eluted protein is 233 kDa as determined by the SLS method (Supplementary Figure 4). These results demonstrate that EcTFE forms a stable $\alpha_2\beta_2$ heterotetrameric complex whose expected molecular mass is about 240 kDa, in good agreement with previous reports [4]. DLS experiments showed that EcTFE has very low polydispersity. Furthermore, CD spectroscopic measurements of EcTFE and subsequent secondary structure calculations show that it is well folded (Figure 2b), consisting of 53% α-helix, 14% β-strand and 33% random coil. EcTFE exhibited a T_m of 51°C as calculated from the CD melting curve.

Oligomeric state and membrane association of anEcTFE

Coexpression of anEcTFE with a His_6-tag on either one of the subunits, resulted in the copurification of the second subunit, not having the His-tag. This shows that a stable complex of the two different

subunits is formed. For anEcTFE, the expression of the β-subunit is much lower when compared to that of the α-subunit. Therefore, for further studies the construct in which the His-tag is at the N-terminus of the β-subunit has been used. In this way the excessively expressed α-subunit is removed during the washing steps of the IMAC column, whereas the anEcTFE complex can subsequently be eluted with an imidazole gradient. After measuring the polydispersity of the purified anEcTFE in several buffers using DLS, 50 mM Tris buffer containing 500 mM NaCl, 5 mM DTT at pH 8.0 was chosen for all further experiments. Subsequently it was found that addition of 10% glycerol and 0.5 % of LDAO detergent significantly reduced the presence of soluble aggregates. This provided the first hint that the anEcTFE complex could be membrane bound. This was further confirmed by the purification of anEcTFE from the membrane fraction. In addition, anEcTFE showed much lower aggregation and higher purity when purified from the membrane fraction. Therefore, the purification protocol was changed, such that anEcTFE was purified from the membrane fraction and solubilized by a variety of detergents. Among them, detergents like DDM, LDAO and $C_{12}E_9$ solubilized anEcTFE from the membrane fraction (Figure 2c). The solubilized anEcTFE eluted between 55 and 65 mL from a 120 mL HiLoad Superdex 200 column (Figure 2a, 2c and Supplementary Figure 3a). The activity measurements of the proteins of the peak fractions showed that anEcTFE purified in the presence of $C_{12}E_9$ had the highest specific activity among the tested detergents (Figure 2e). The purified protein sample was also tested by BN-PAGE to identify the oligomeric state and molecular mass of the complex. In all experiments with the various detergents, the mobility of the anEcTFE major band corresponded to the position of the 480 kDa marker. There were also higher oligomers present in DDM, LDAO and $C_{12}E_9$ (Figure 2f and Supplementary Figure 3c-d). Further DLS measurements showed that the protein solubilized in $C_{12}E_9$ has the lowest polydispersity among the tested detergents. Therefore, $C_{12}E_9$ was chosen as the most suitable detergent to solubilize anEcTFE from the membrane fraction and for further purification steps. The molecular mass of the protein of the peak fractions eluted in the buffer containing $C_{12}E_9$ was further determined by SLS to be about 535 kDa (Supplementary Figure 4). These results show that anEcTFE purified under these conditions corresponds to an octamer, most likely a dimer of two $\alpha_2\beta_2$ heterotetramers. CD spectroscopic measurements of anEcTFE (Figure 2b) and subsequent secondary structure calculations show that it is well folded consisting of 40% α-helix, 30% β-strand and 30% random coil. CD melting curve measurements showed that the T_m of anEcTFE is 49 °C.

Oligomeric state of HsTFE

HsTFE was purified as a complex of α- and β- subunits by the IMAC technique using a His_6-tag at the N-terminus of the β-subunit. Previous studies [48] have clearly shown that HsTFE is a

mitochondrial inner membrane associated complex and therefore detergent was used throughout the purification to solubilize the complex. Different detergents such as LDAO, DDM, $C_{12}E_9$, β-OG, CYMAL-6, DMNG and CHAPS were tested in the purification of HsTFE for getting a monodisperse protein sample. Among them, LDAO, DDM, $C_{12}E_9$, β-OG and CYMAL-6 solubilized the HsTFE complex. However, the eluted peaks during SEC were not very symmetrical, suggesting the presence of different oligomeric species of HsTFE as also seen in the BN-PAGE experiment. The peaks of the HsTFE solubilized in LDAO, DDM, CYMAL-6 and β-OG eluted from 11.5 to 12.5 mL whereas the peak of HsTFE solubilized in $C_{12}E_9$ eluted at 11 mL in a 24 mL SEC column. HsTFE elutes at 60.5 mL when using a Superdex 200 Hiload 16/60 column (120mL) (Figure 2a and Supplementary Figure 3b). The CD experiment (Figure 2b) suggests that the protein is folded consisting of 30% α-helix, 25% β-strand and 45% random coil. HsTFE also exhibited a T_m of 51 °C in CD melting curve. Furthermore, the purified sample was tested for the overall activity of the HsTFE-α subunit (HAD activity) at 340 nm and HsTFE exhibits maximum activity when it is solubilized in the presence of $C_{12}E_9$ as shown in Figure 2e. The BN-PAGE experiment suggests that the HsTFE sample is a mixture of heterotetrameric, heterooctameric and other higher oligomeric species. A mixture of heterotetrameric and heterooctameric assemblies was also observed in previous studies [15,16,48]. However, the octameric band of about 500 kDa is more prominent in the $C_{12}E_9$ solubilized sample, suggesting that HsTFE is predominantly heterooctameric in the presence of $C_{12}E_9$ (Figure 2f and Supplementary Figure 3e). The SLS experiment with the HsTFE complex solubilized in the presence of $C_{12}E_9$ showed that the molecular mass of the complex is about 580 kDa which is close to its heterooctameric molecular mass (Supplementary Figure 4). Although β-OG and DDM have been used to solubilize the HsTFE complex in other studies [15,16,48], in the studies reported here, the best results were obtained with $C_{12}E_9$, being based on the measurements concerning the HsTFE catalytic activity, the symmetry of its SEC peak and the lower polydispersity of this sample.

Substrate preferences for EcTFE, anEcTFE and HsTFE

The ECH and HAD specific activities of EcTFE, anEcTFE and HsTFE were determined for a range of fatty acyl-CoA substrates. For both assays the used substrate is the corresponding *2E*-enoyl-CoA. The hydratase activity is measured in a direct assay in which the disappearance of the double bond is monitored spectrophotometrically at 263 nm. The dehydrogenase activity is measured in a linked assay in which the substrate is generated by the TFE-hydratase active site and CoA is included in the

assay buffer such that the 3-ketoacyl-CoA product of the dehydrogenase reaction is immediately converted further by the TFE thiolase active site, avoiding product inhibition [49]. Product formation in the latter assay is measured spectrophotometrically at 340 nm by measuring the formation of NADH. The substrates tested were linear short, medium and long chain enoyl-CoAs such as *2E*-butenoyl-CoA, *2E*-decenoyl-CoA and *2E*-hexadecenoyl-CoA (Figure 3a). In addition, 2-methyl branched enoyl-CoAs such as 2-methyl-*2E*-decenoyl-CoA and pristenoyl-CoA as well as bulky enoyl-CoAs such as *24E*-THCe-CoA (which is also 2-methyl branched), and its unmethylated variant (*24E*,25DM-THCe-CoA) were used as substrates. Among the tested substrates, EcTFE showed detectable activity with *2E*-butenoyl-CoA, *2E*-decenoyl-CoA, *2E,4E*-decadienoyl-CoA and *2E*-hexadecenoyl-CoA. Of these, *2E*-butenoyl-CoA showed highest specific activity for both the ECH as well as the HAD reaction, followed by *2E*-decenoyl-CoA and then by *2E*-hexadecenoyl-CoA (Figure 3b). EcTFE showed very low activity with *2E,4E*-decadienoyl-CoA. However, there was no detectable activity with the 2-methyl-branched enoyl-CoAs and with the bulky enoyl-CoAs. These results show that EcTFE accepts only linear, non-branched enoyl-CoAs as substrates with a preference for short chain enoyl-CoAs over longer chain enoyl-CoAs. anEcTFE and HsTFE exhibited highest specific activity for the ECH and HAD reactions with *2E*-decenoyl-CoA at 60 µM substrate concentration (Figure 3b). However, at lower substrate concentrations (below 60 µM) both anEcTFE and HsTFE exhibited highest activity with *2E*-hexadecenoyl-CoA in both the hydratase as well as the dehydrogenase assay, suggesting that at 60 µM concentration of *2E*-hexadecenoyl-CoA, micelle formation of the substrate affects the assay results. anEcTFE as well as HsTFE showed very low ECH and HAD activity with *2E*-butenoyl-CoA, *2E,4E*-decadienoyl-CoA, 2-methyl-*2E*-decenoyl-CoA and no detectable activity with pristenoyl-CoA, *24E*-THCe-CoA and *24E*,25DM-THCe-CoA (Figure 3b). anEcTFE and HsTFE show KAT activity with *2E*-decenoyl-CoA and *2E*-hexadecenoyl-CoA in a qualitative assay. For EcTFE the measured KAT activity with these substrates is very low. Only EcTFE exhibited measurable KAT activity (specific activity of 0.5 ± 0.03 µmole mg^{-1} min^{-1}) with acetoacetyl-CoA. These results show that all three active sites of anEcTFE and HsTFE can degrade long chain linear (non-bulky) enoyl-CoAs as substrates, whereas all three active sites of EcTFE can degrade short chain linear substrates.

Since only the linear enoyl-CoAs showed considerable activity with all three TFEs, the apparent Michaelis-Menten constants for the ECH and HAD active sites were also determined with *2E*-butenoyl-CoA, *2E*-decenoyl-CoA and *2E*-hexadecenoyl-CoA (Table 1). The catalytic efficiency (k_{cat}/K_m) of the ECH active site of EcTFE with *2E*-butenoyl-CoA is 10-20 fold higher than when *2E*-decenoyl-CoA or *2E*-hexadecenoyl-CoA are used as substrates. The HAD active site of EcTFE shows

higher k_{cat} for 3S-hydroxybutanoyl-CoA when compared to 3S-hydroxydecanoyl-CoA or 3S-hydoxyhexadecanoyl-CoA. The overall catalytic efficiency, expressed as the k_{cat}/K_m-value, of the EcTFE HAD active sites is almost the same for all three tested substrates (Table 1), but the K_m value of the short chain substrate is much higher and therefore the short chain substrate is more efficiently degraded [50]. For anEcTFE and HsTFE, the apparent Michaelis-Menten constants were measured only with *2E*-decenoyl-CoA and *2E*-hexadecenoyl-CoA as substrates (Table 1) because saturation kinetics was not observed with *2E*-butenoyl-CoA although some low ECH activity is measured at higher substrate concentrations. The ECH and HAD catalytic efficiency of anEcTFE is higher for *2E*-hexadecenoyl-CoA as compared to that for *2E*-decenoyl-CoA. The ECH and HAD catalytic efficiency of HsTFE is comparable for both *2E*-decenoyl-CoA and *2E*-hexadecenoyl-CoA (Table 1).

In previous studies the k_{cat} and K_m values for the ECH and HAD activities of the endogenously expressed EcTFE for the *2E*-decenoyl-CoA substrate [4] have been reported. Also the Michaelis-Menten kinetic parameters of the endogenously expressed porcine TFE (like HsTFE this is the mitochondrial TFE) have been reported, but only for the *2E*-hexadecenoyl-CoA substrate [20]. The pH of the assay buffers in these assays (also done at 25 ^{o}C) was pH 8, whereas in the current studies the pH is 9. In the previous EcTFE studies the ECH assay and the HAD assay were indirect assays, employing various linker enzymes. Nevertheless the K_m values are in the same range, but the k_{cat} values are higher. For the porcine TFE [20] also the k_{cat} and K_m values for the overall reaction, measured without employing linker enzymes in the assay mixture, were reported for *2E*-hexadecenoyl-CoA and in this assay mixture the k_{cat} is approximately 2.3 s^{-1}, with K_m of 2.7 μM. These values are similar as observed here (Table 1), being 2.5 s^{-1} and 0.9 μM, respectively. In any case, the studies reported here have been aimed at comparing the catalytic properties of the three different TFEs with each other and for substrates of different chain lengths and the results show that EcTFE can metabolize efficiently short chain linear fatty acyl-CoA substrates whereas anEcTFE and HsTFE can only degrade medium to long chain linear fatty acyl-CoA substrates efficiently.

SAXS studies of the EcTFE heterotetramer

The SAXS data for EcTFE were collected in HPLC mode. The Kratky analysis of the experimental data suggests that the protein is well folded (Figure 4a). The R_g and D_{max} as calculated by the SCATTER and PRIMUS (ATSAS) programs was 46 and 160 Å, respectively (Figure 4b). The

molecular mass of EcTFE estimated with the Size&Shape method from the SAXS experiment was 248 kDa, which is very close to the expected molecular mass of heterotetrameric EcTFE (Table 2). PfTFE is a close homolog of EcTFE, therefore the individual α- and β-subunits of EcTFE were modeled using the SWISS-MODEL server and using the corresponding subunits of PfTFE (PDB code: 1WDM) as reference model. Subsequently, the EcTFE heterotetrameric assembly was generated, by superposing the respective models of the individual subunits on the PfTFE tetramers. The secondary structure composition of the model as calculated by STRIDE is 48% α-helix, 15% β-strand and 37% random coil which is very similar to the values obtained from CD experiment. The built EcTFE heterotetramer model was fitted to the EcTFE experimental SAXS data using the programs FoXS and CRYSOL resulting in a χ^2 value of 2.74 and 1.35 respectively (Figure 4c and Table 2). Moreover, EcTFE and PfTFE belong to the same TFE subfamily [14], and the individual subunits of EcTFE share about 60% sequence identity with the corresponding subunits of PfTFE, predicting that the EcTFE and the PfTFE assembly will be similar. Indeed, the SAXS *ab initio* shape of EcTFE as generated by the program DAMMIN as well as the low-resolution electron density map generated by the DENSSWeb server from the experimental EcTFE SAXS scattering data, show that the EcTFE tetrameric assembly resembles the PfTFE tetramer (Figure 4d and 4e).

SAXS studies of the anEcTFE heterooctamer

The SAXS data were collected for anEcTFE in the presence of $C_{12}E_9$ in HPLC mode. The data do not show any clear signs of a detergent micellar scattering contribution, which was confirmed for the atomic model described below by fitting a linear combination of the scattering from the atomic structure and of the scattering of detergent micelles. The Kratky analysis of the experimental data suggests that this complex is well folded (Figure 5a). The R_g and D_{max} as calculated by the SCATTER as well as the PRIMUS (ATSAS) programs was 61 Å and 196 Å, respectively (Figure 5b). The molecular mass of anEcTFE estimated with the Size&Shape method from the SAXS data was 521 kDa, which is close to the expected molecular mass of heterooctameric anEcTFE (Table 2). Previous bioinformatics studies suggest that the anEcTFE α- and β- subunit sequences are more closely related to the mitochondrial TFE (HsTFE) subfamily than to other bacterial TFE subfamilies [14]. anEcTFE and HsTFE share about 38 % and 37.5 % sequence identity for the α and β subunits respectively, whereas the sequence identity between the anEcTFE and EcTFE subunits is 34.5 % and 33.5 %. During the preparation of this manuscript, the cryoEM structure of HsTFE (PDB code: 5ZQZ) was reported [15], and more recently also it's crystal structure (PDB code: 6DV2) [16]. There is good agreement between these structures showing that HsTFE is also a $\alpha_2\beta_2$- heterotetramer. The individual

α- and β-subunits of anEcTFE were therefore modeled with the SWISS-MODEL server using the corresponding subunits of HsTFE (PDB code: 5ZQZ) as the reference. Subsequently, the anEcTFE heterotetrameric assembly was generated, by superposing the respective modeled individual subunits on the HsTFE tetramer. The *ab initio* shape of anEcTFE was generated from the SAXS data using the DAMMIN program. This *ab initio* shape clearly suggested that it can accommodate a complex bigger than the tetrameric TFE. In addition, SEC, SLS as well as BN-PAGE experiments also suggest that anEcTFE is a heterooctamer. In all the three known TFE structures (PfTFE, MtTFE and HsTFE), the basic assembly is a heterotetramer. In HsTFE the octameric form (PDB code: 5ZRV) is a loose assembly of two tetramers, being stabilized via hydrophobic interactions mediated by lipid molecules. The heterooctameric assembly of anEcTFE was generated by superposing the respective modeled individual anEcTFE subunits on the HsTFE octamer subunits. Both the anEcTFE heterotetramer as well as the anEcTFE heterooctamer atomic model did not match with the experimental anEcTFE SAXS data when analyzed by the FoXS and CRYSOL programs (χ^2 is 175 and 55 for the heterotetramer and heterooctamer model respectively in FoXS) (Figure 5c). Therefore, different octameric models were generated by moving one anEcTFE tetramers with respect to the other, in such a way that a better fit is achieved with the calculated shape. All the generated heterooctameric assemblies were fitted to the experimental anEcTFE SAXS data using FoXS and CRYSOL program. The anEcTFE heterooctameric assembly with the best fit to the SAXS yielded a χ^2 value of 3.50 as shown in Figure 5c and Table 2. The secondary structure composition of the anEcTFE model, having 37% α-helix, 16% β-strand and 47% random coil, suggests a predominant helical content as also predicted from the CD-experiment. The heterooctameric model was superimposed on the *ab initio* shape of anEcTFE as shown in Figure 5d and the model fits reasonably well in the shape. This octameric model also fitted well in the electron density map that was generated from the experimental SAXS data of anEcTFE by the DENSSWeb server (Figure 5e).

EM studies of EcTFE and anEcTFE

The particles picked from the EM micrographs were processed using the RELION software. The glutaraldehyde crosslinked EcTFE sample was used, therefore there were several joined double particles which were visible from the 1D micrograph and 2D classes (Figure 6a). These particles/classes were not used for the 3D classification. The final 3D map of EcTFE was calculated by the 3D autorefine module of RELION to a resolution of 24 Å. The final 3D-EM map of EcTFE very much resembled the PfTFE tetramer assembly (Figure 6c). The anEcTFE 3D-EM map (23 Å resolution) was calculated in a similar way. The anEcTFE heterooctamer model, as obtained from the

SAXS fitting, also fits well to the 3D-EM map calculated from the EM images. These data clearly suggest that anEcTFE has a heterooctameric structure, where the α and β subunits are assembled in a heterotetramer very similar as in the assembly of the α and β subunits in the HsTFE heterotetramer structure (Figure 6 d-f). The final 3D-EM maps of EcTFE and anEcTFE match well with the electron density maps of respectively EcTFE and anEcTFE, as generated from the experimental SAXS data using the DENSSWeb program (Figure 4e and 6c for EcTFE and Figure 5e and 6f for anEcTFE).

Discussion

A unique property of the enzyme systems of the fatty acid degradation pathway is their broad substrate specificity with respect to the chain length of the fatty acyl moieties conjugated to CoA. Evolution has found several solutions to achieve this broad substrate specificity. Such β-oxidation enzyme systems efficiently degrade long chain fatty acids completely to acetyl-CoA and reducing equivalents and in this way the free energy required to activate the fatty acids to the acyl-CoA conjugates is fully used [1]. At the molecular level, this broad chain length specificity can be achieved in different ways. For example, for the monofunctional mitochondrial ECH, the acyl chain binding pocket is closed when complexed with short chain fatty acyl-CoA molecules, like acetoacetyl-CoA [51], whereas the covering lid of the binding pocket becomes disordered when being complexed with longer chain fatty acyl-CoA molecules, like octanoyl-CoA [52]. In other enzymes the short and long chain acyl tails bind in a preformed tunnel. In the ECH active site of the MFE1 this tunnel connects the catalytic site with bulk solvent and the longer chain acyl tails point into bulk solvent without rearrangements of the residues shaping this binding pocket [53,54], whereas in acyl-CoA dehydrogenases such a tunnel is an extended, buried pocket [11,55]. In the latter example evolutionary pressure has generated also different subfamilies of dehydrogenases with complementary substrate specificity. The systematic kinetic analysis of anEcTFE and EcTFE reported here shows that EcTFE and anEcTFE also have complementary substrate specificity, being that EcTFE preferentially degrades short chain, linear enoyl-CoAs, whereas anEcTFE preferentially degrades medium and long chain, linear enoyl-CoA substrates. The functional role of anEcTFE in the *E. coli* lipid metabolism is not fully understood. It appears that anEcTFE is essential for the anaerobic degradation of fatty acids in the presence of nitrate as electron acceptor [1,6]. Under anaerobic conditions, the expression of EcTFE is repressed by ArcA even in the presence of long chain fatty acids while anEcTFE is still expressed [56]. However, under aerobic conditions both EcTFE and anEcTFE are expressed and are functional. For example, in *E. coli* knockout studies in which the FadB gene (coding for EcTFE-α) has been deleted, it is found that this strain can still catalyze chain length reduction of long chain fatty acids by FadJ (coding for anEcTFE-α), as is required for the synthesis of PHAs [5]. This suggests that, under aerobic conditions

EcTFE and anEcTFE jointly contribute to the complete degradation of long chain fatty acids to produce acetyl-CoA and reducing equivalents, and therefore the free energy required to activate the fatty acids to their acyl-CoA conjugates is fully used [1]. Under anaerobic conditions the degradation of fatty acids by only ydiO (Figure 1) and anEcTFE is less efficient, generating predominantly short chain acyl-CoA products. In the evolution of cellular metabolism, the anaerobic metabolism has developed first, whereas the development of the aerobic metabolism came later, being triggered by the appearance of oxygen once photosynthesis pathways had emerged. This suggests that the soluble EcTFE evolved from anEcTFE as an adaptation, allowing, together with acyl-CoA dehydrogenase (FadE, Figure 1), for a more efficient degradation of the available fatty acids.

It is also interesting to note that EcTFE and anEcTFE exhibit different structural properties whereas anEcTFE and HsTFE share several common structural features as shown in this study. EcTFE is purified as a soluble, heterotetrameric assembly, in the absence of any detergent. The SAXS and EM studies reported here, show that the EcTFE heterotetrameric assembly is similar to the PfTFE heterotetrameric assembly, which is consistent with the previous suggestion that PfTFE and EcTFE are in the same TFE-subfamily. In contrast, SEC, SLS and BN-PAGE experiments show that anEcTFE is predominantly a heterooctameric complex, probably a dimer of two heterotetramers. Although previously anEcTFE has been purified in the absence of detergent (but in the presence of 20% glycerol) [5], the studies reported here show that anEcTFE is membrane bound. Like in *E. coli*, also in the mitochondrial fatty acid degradation system two β-oxidation pathways exist, being the membrane associated enzymes and the soluble monofunctional enzymes. The membrane associated mitochondrial VLCAD and TFE (for example, HsTFE) catalyze the first and the last three steps of the β-oxidation cycle of the very-long-chain acyl-CoAs, respectively ([11,48] and this study), while in the soluble system, the reactions on shorter acyl-CoAs are catalyzed by the soluble monofunctional enzymes [57]. In this respect it is interesting that the phylogenetic sequence analysis shows that the α and β subunits of HsTFE are more closely related to anEcTFE than to EcTFE [14,17]. Moreover, the sequence alignments (Supplementary Figures 1 and 2) show that anEcTFE as well as HsTFE have very similar insertions and deletions in their sequences when compared to other TFE sequences. The only major difference between the anEcTFE and HsTFE sequences is in the α-subunit, between residues Pro224 and Ile237 (Insertion 1 in HsTFE-α, Supplementary Figure 1). This loop is shorter in anEcTFE compared to HsTFE. Therefore, the structures of the individual subunits of anEcTFE, as modeled using the HsTFE subunits as templates, make a HsTFE-like tetrameric assembly without any clashes between the subunits. The interactions between the tetramers in the HsTFE octamer are mediated by hydrophobic interactions [15], suggesting that the formation of the octamer is a

purification artefact caused by disrupting the *in vivo* interactions between the tetramer and the membrane. Interestingly, the HsTFE octamer as determined from cryoEM studies by Liang and coworkers, is too large to fit into the electron density shape of anEcTFE calculated from the EM and SAXS data. Therefore, a new octameric assembly is proposed for anEcTFE which fits well to both SAXS as well as EM data. One of the anEcTFE tetramers fits very well to the observed density, significantly better than the second tetramer (Figure 6f). It is possible that there is still some heterogeneity in the selected anEcTFE set of molecules. Noteworthy, a second octamer population observed in the HsTFE cryoEM studies [15], resembles the shape of anEcTFE better, but further analysis of this population was not reported. The anEcTFE octameric model is more compact, suggesting that there are only few detergent molecules between the two anEcTFE tetramers.

In conclusion, the enzyme kinetic data and the sequence and structural data reported here suggest that the anEcTFE and HsTFE are evolutionarily more closely related to each other than to EcTFE. They also have similar functions, being the β-oxidation of (very) long chain acyl-CoA molecules. The assemblies of EcTFE and anEcTFE are different, therefore the underlying mechanism of substrate channeling will be different in these two TFEs, especially the channeling between the α- and β-subunits. Kinetic data suggest that EcTFE [4] and HsTFE [20] have substrate channeling properties and for PfTFE, a close homolog of EcTFE, a substrate channeling mechanism has been proposed [13]. We speculate that the substrate channeling mechanisms in EcTFE and anEcTFE will be similar to those in PfTFE and HsTFE, respectively. Further studies towards the detailed structural and enzymological properties of EcTFE and anEcTFE have been initiated to understand better the reaction mechanisms and the substrate channeling properties of the two *E. coli* β-oxidation enzyme systems.

Data availability

The SAXS data, *ab initio* shapes and molecular models for EcTFE as well as for anEcTFE have been deposited in the small angle scattering biological data bank (SASBDB) with accession code: SASDEL9 and SASDEM9 for EcTFE and anEcTFE, respectively. The 3D-EM maps of the EcTFE and anEcTFE samples are available from the corresponding author on request. All other data generated or analyzed during this study are included in this published article and/or in its supplementary information document.

Acknowledgements

We acknowledge Biocenter Oulu core facilities (proteomics and protein analysis, DNA sequencing, Electron Microscopy and protein X-ray crystallography (also supported by Biocenter Finland and Instruct-FI)) and Biocenter Finland EM core facility at Helsinki. We appreciate the help of Pasi A.

Laurinmäki and Dr. Bishal Kumar Singh for the help with the collection and processing of the negative staining EM data, respectively. We thank the beam line scientists at DLS and ESRF for their expert support and Prof. Kalervo J. Hiltunen for scientific discussions.

Competing interests

The authors declare that they have no competing interests.

Funding

The work was funded by the Academy of Finland grants to SS (293369) and to RV (289024). The work was also supported by a grant from the Faculty of Biochemistry and Molecular Medicine, University of Oulu to SS.

Author contributions

SS performed all cloning, purification, kinetic and structural studies. RV and SS collected SAXS and EM data. MH purified EcTFE for kinetic and structural studies. WS synthesized all the fatty acyl-CoA substrates used in this work. JSP analyzed SAXS data for detergent micellar contribution. JAG, JS and SJB assisted in the processing and analysis of the negative staining EM data. SS, RKW and RV designed the experiments, analyzed all the data and wrote the manuscript with comments from all other authors.

References

1. Campbell, J. W., Morgan-Kiss, R. M. and Cronan Jr., J. E. (2003) A new escherichia coli metabolic competency: Growth on fatty acids by a novel anaerobic b-oxidation pathway. Mol. Microbiol. **47**, 793-805. doi:10.1046/j.1365-2958.2003.03341.x

2. Feigenbaum Binstock, J., Pramanik, A. and Schulz, H. (1977) Isolation of a multi enzyme complex of fatty acid oxidation from escherichia coli. Proc. Natl. Acad. Sci. U. S. A. **74**, 492-495

3. Pramanik, A., Pawar, S., Antonian, E. and Schulz, H. (1979) Five different enzymatic activities are associated with the multienzyme complex of fatty acid oxidation from escherichia coli. J. Bacteriol. **137**, 469-473

4. Yang, S. -., Bittman, R. and Schulz, H. (1985) Channeling of a β-oxidation intermediate on the large subunit of the fatty acid oxidation complex from escherichia coli. J. Biol. Chem. **260**, 2862-2868

5. Snell, K. D., Feng, F., Zhong, L., Martin, D. and Madison, L. L. (2002) YfcX enables medium-chain-length poly(3-hydroxyalkanoate) formation from fatty acids in recombinant escherichia coli fadB strains. J. Bacteriol. **184**, 5696-5705. doi:10.1128/JB.184.20.5696-5705.2002

6. Gulevich, A. Y., Skorokhodova, A. Y. and Debabov, V. G. (2016) Escherichia coli ydiO and ydiQRST genes encode components of acyl-CoA dehydrogenase complex of anaerobic fatty acid ß-oxidation pathway. Genetika. **52**, 1210-1214

7. Tappel, R. C., Wang, Q. and Nomura, C. T. (2012) Precise control of repeating unit composition in biodegradable poly(3-hydroxyalkanoate) polymers synthesized by escherichia coli. J. Biosci. Bioeng. **113**, 480-486. doi:10.1016/j.jbiosc.2011.12.004

8. Olivera, E. R., Carnicero, D., García, B., Miñambres, B., Moreno, M. A., Cañedo, L., DiRusso, C. C., Naharro, G. and Luengo, J. M. (2001) Two different pathways are involved in the ß-oxidation of n-alkanoic and n-phenylalkanoic acids in pseudomonas putida U: Genetic studies and biotechnological applications. Mol. Microbiol. **39**, 863-874. doi:10.1046/j.1365-2958.2001.02296.x

9. Jones, S. A., Gibson, T., Maltby, R. C., Chowdhury, F. Z., Stewart, V., Cohen, P. S. and Conway, C. (2011) Anaerobic respiration of escherichia coli in the mouse intestine. Infect. Immun. **79**, 4218-4226. doi:10.1128/IAI.05395-11

10. Segura, A., Bertoni, M., Auffret, P., Klopp, C., Bouchez, O., Genthon, C., Durand, A., Bertin, Y. and Forano, E. (2018) Transcriptomic analysis reveals specific metabolic pathways of enterohemorrhagic escherichia coli O157:H7 in bovine digestive contents 06 biological sciences 0604 genetics. BMC Genomics. **19**. doi:10.1186/s12864-018-5167-y

11. McAndrew, R. P., Wang, Y., Mohsen, A. -., He, M., Vockley, J. and Kim, J. -. P. (2008) Structural basis for substrate fatty acyl chain specificity: Crystal structure of human very-long-chain acyl-CoA dehydrogenase. J. Biol. Chem. **283**, 9435-9443. doi:10.1074/jbc.M709135200

12. Uchida, Y., Izai, K., Orii, T. and Hashimoto, T. (1992) Novel fatty acid ß-oxidation enzymes in rat liver mitochondria: II. purification and properties of enoyl-coenzyme A (CoA) hydratase/3-

hydroxyacyl-CoA dehydrogenase/3-ketoacyl-CoA thiolase trifunctional protein. J. Biol. Chem. **267**, 1034-1041

13. Ishikawa, M., Tsuchiya, D., Oyama, T., Tsunaka, Y. and Morikawa, K. (2004) Structural basis for channelling mechanism of a fatty acid ß-oxidation multienzyme complex. EMBO J. **23**, 2745-2754. doi:10.1038/sj.emboj.7600298

14. Venkatesan, R. and Wierenga, R. K. (2013) Structure of mycobacterial ß-oxidation trifunctional enzyme reveals its altered assembly and putative substrate channeling pathway. ACS Chem. Biol. **8**, 1063-1073. doi:10.1021/cb400007k

15. Liang, K., Li, N., Wang, X., Dai, J., Liu, P., Wang, C., Chen, X. -., Gao, N. and Xiao, J. (2018) Cryo-EM structure of human mitochondrial trifunctional protein. Proc. Natl. Acad. Sci. U. S. A. **115**, 7039-7044. doi:10.1073/pnas.1801252115

16. Chuanwu Xia, Zhuji Fu, Kevin P. Battaile, Jung-Ja P. Kim. (2019) Crystal structure of human mitochondrial trifunctional protein, a fatty acid β-oxidation metabolon. Proceedings of the National Academy of Sciences of the United States of America. **116**, 6069-6074. doi:10.1073/pnas.1816317116

17. Anbazhagan, P., Harijan, R. K., Kiema, T. R., Janardan, N., Murthy, M. R. N., Michels, P. A. M., Juffer, A. H. and Wierenga, R. K. (2014) Phylogenetic relationships and classification of thiolases and thiolase-like proteins of mycobacterium tuberculosis and mycobacterium smegmatis. Tuberculosis. **94**, 405-412. doi:10.1016/j.tube.2014.03.003

18. Stanley, K. K. and Tubbs, P. K. (1975) The role of intermediates in mitochondrial fatty acid oxidation. Biochem. J. **150**, 77-88. doi:10.1042/bj1500077

19. Nada, M. A., Rhead, W. J., Sprecher, H., Schulz, H. and Roe, C. R. (1995) Evidence for intermediate channeling in mitochondrial ß-oxidation. J. Biol. Chem. **270**, 530-535. doi:10.1074/jbc.270.2.530

20. Yao, K. -. and Schulz, H. (1996) Intermediate channeling on the trifunctional ß-oxidation complex from pig heart mitochondria. J. Biol. Chem. **271**, 17816-17820. doi:10.1074/jbc.271.30.17816

21. Vögeli, B., Engilberge, S., Girard, E., Riobé, F., Maury, O., Erb, T. J., Shima, S. and Wagner, T. (2018) Archaeal acetoacetyl-CoA thiolase/HMG-CoA synthase complex channels the intermediate via a fused CoA-binding site. Proc. Natl. Acad. Sci. U. S. A. **115**, 3380-3385. doi:10.1073/pnas.1718649115

22. Bernhardsgrütter, I., Vögeli, B., Wagner, T., Peter, D. M., Cortina, N. S., Kahnt, J., Bange, G., Engilberge, S., Girard, E., Riobé, F., Maury, O., Shima, S., Zarzycki, J. and Erb, T. J. (2018) The multicatalytic compartment of propionyl-CoA synthase sequesters a toxic metabolite. Nat. Chem. Biol. **14**, 1127-1132. doi:10.1038/s41589-018-0153-x

23. Ishikawa, M., Mikami, Y., Usukura, J., Iwasaki, H., Shinagawa, H. and Morikawa, K. (1997) Reconstitution, morphology and crystallization of a fatty acid ß-oxidation multienzyme complex from pseudomonas fragi. Biochem. J. **328**, 815-820. doi:10.1042/bj3280815

24. Cohen, R. D. and Pielak, G. J. (2017) A cell is more than the sum of its (dilute) parts: A brief history of quinary structure. Protein Sci. **26**, 403-413. doi:10.1002/pro.3092

25. Yang, S. -., Cuebas, D. and Schulz, H. (1986) 3-hydroxyacyl-CoA epimerases of rat liver peroxisomes and escherichia coli function as auxiliary enzymes in the ß-oxidation of polyunsaturated fatty acids. J. Biol. Chem. **261**, 12238-12243

26. Lin, J. -., Palomec, L. and Wheeldon, I. (2014) Design and analysis of enhanced catalysis in scaffolded multienzyme cascade reactions. ACS Catal. **4**, 505-511. doi:10.1021/cs401009z

27. Wittig, I., Braun, H. -. and Schägger, H. (2006) Blue native PAGE. Nat. Protoc. **1**, 418-428. doi:10.1038/nprot.2006.62

28. Schmitz, W., Fingerhut, R. and Conzelmann, E. (1994) Purification and properties of an a-methylacyl-CoA racemase from rat liver. Eur. J. Biochem. **222**, 313-323. doi:10.1111/j.1432-1033.1994.tb18870.x

29. Bal, B. S., Childers Jr., W. E. and Pinnick, H. W. (1981) Oxidation of a,ß-un saturated aldehydes. Tetrahedron. **37**, 2091-2096. doi:10.1016/S0040-4020(01)97963-3

30. Pedersen, J. S. (2004) A flux- and background-optimized version of the NanoSTAR small-angle X-ray scattering camera for solution scattering. J. Appl. Crystallog. **37**, 369-380. doi:10.1107/S0021889804004170

31. Förster, S., Apostol, L. and Bras, W. (2010) Scatter: Software for the analysis of nano-and mesoscale small-angle scattering. J. Appl. Crystallog. **43**, 639-646. doi:10.1107/S0021889810008289

32. Konarev, P. V., Volkov, V. V., Sokolova, A. V., Koch, M. H. J. and Svergun, D. I. (2003) PRIMUS: A windows PC-based system for small-angle scattering data analysis. J. Appl. Crystallog. **36**, 1277-1282. doi:10.1107/S0021889803012779

33. Svergun, D. I. (1992) Determination of the regularization parameter in indirect-transform methods using perceptual criteria. J Appl Crystallogr. **25**, 495-503. doi:10.1107/S0021889892001663

34. Hajizadeh, N. R., Franke, D., Jeffries, C. M. and Svergun, D. I. (2018) Consensus bayesian assessment of protein molecular mass from solution X-ray scattering data. Sci. Rep. **8**. doi:10.1038/s41598-018-25355-2

35. Svergun, D. I. (1999) Restoring low resolution structure of biological macromolecules from solution scattering using simulated annealing. Biophys. J. **76**, 2879-2886. doi:10.1016/S0006-3495(99)77443-6

36 . Franke, D. and Svergun, D. I. (2009) DAMMIF, a program for rapid ab-initio shape determination in small-angle scattering. J. Appl. Crystallog. **42**, 342-346. doi:10.1107/S0021889809000338

37. Grant, T. D. (2018) Ab initio electron density determination directly from solution scattering data. Nat. Methods. **15**, 191-193. doi:10.1038/nmeth.4581

38. Schneidman-Duhovny, D., Hammel, M., Tainer, J. A. and Sali, A. (2013) Accurate SAXS profile computation and its assessment by contrast variation experiments. Biophys. J. **105**, 962-974. doi:10.1016/j.bpj.2013.07.020

39. Svergun, D., Barberato, C. and Koch, M. H. (1995) CRYSOL - A program to evaluate X-ray solution scattering of biological macromolecules from atomic coordinates. J. APPL. CRYSTALLOGR. **28**, 768-773. doi:10.1107/S0021889895007047

40. Steiner, E. M., Lyngsø, J., Guy, J. E., Bourenkov, G., Lindqvist, Y., Schneider, T. R., Pedersen, J. S., Schneider, G. and Schnell, R. (2018) The structure of the N-terminal module of the cell wall hydrolase RipA and its role in regulating catalytic activity. Proteins Struct. Funct. Bioinformatics. **86**, 912-923. doi:10.1002/prot.25523

41. Pettersen, E. F., Goddard, T. D., Huang, C. C., Couch, G. S., Greenblatt, D. M., Meng, E. C. and Ferrin, T. E. (2004) UCSF chimera - A visualization system for exploratory research and analysis. J. Comput. Chem. **25**, 1605-1612. doi:10.1002/jcc.20084

42. Schwede, T., Kopp, J., Guex, N. and Peitsch, M. C. (2003) SWISS-MODEL: An automated protein homology-modeling server. Nucleic Acids Res. **31**, 3381-3385. doi:10.1093/nar/gkg520

43. Krissinel, E. and Henrick, K. (2004) Secondary-structure matching (SSM), a new tool for fast protein structure alignment in three dimensions. Acta Crystallogr. Sect. D Biol. Crystallogr. **60**, 2256-2268. doi:10.1107/S0907444904026460

44. Emsley, P. and Cowtan, K. (2004) Coot: Model-building tools for molecular graphics. Acta Crystallogr. Sect. D Biol. Crystallogr. **60**, 2126-2132. doi:10.1107/S0907444904019158

45. Frishman, D. and Argos, P. (1995) Knowledge-based protein secondary structure assignment. Proteins Struct. Funct. Genet. **23**, 566-579. doi:10.1002/prot.340230412

46. Tang, G., Peng, L., Baldwin, P. R., Mann, D. S., Jiang, W., Rees, I. and Ludtke, S. J. (2007) EMAN2: An extensible image processing suite for electron microscopy. J. Struct. Biol. **157**, 38-46. doi:10.1016/j.jsb.2006.05.009

47. Scheres, S. H. W. (2012) RELION: Implementation of a bayesian approach to cryo-EM structure determination. J. Struct. Biol. **180**, 519-530. doi:10.1016/j.jsb.2012.09.006

48. Fould, B., Garlatti, V., Neumann, E., Fenel, D., Gaboriaud, C. and Arlaud, G. J. (2010) Structural and functional characterization of the recombinant human mitochondrial trifunctional protein. Biochemistry. **49**, 8608-8617. doi:10.1021/bi100742w

49. He, X. -., Yang, S. -. and Schulz, H. (1992) Inhibition of enoyl-CoA hydratase by long-chain l-3-hydroxyacyl-CoA and its possible effect on fatty acid oxidation. Arch. Biochem. Biophys. **298**, 527-531. doi:10.1016/0003-9861(92)90445-3

50. Fersht Alan. (2017) Structure and mechanism in protein science : A guide to enzyme catalysis and protein folding. series in structural biology -vol.9. , World Scientific publishing Co. Pvt. Ltd., Singapore

51. Engel, C. K., Mathieu, M., Zeelen, J. P., Hiltunen, J. K. and Wierenga, R. K. (1996) Crystal structure of enoyl-coenzyme A (CoA) hydratase at 2.5 Å resolution: A spiral fold defines the CoA-binding pocket. EMBO J. **15**, 5135-5145

52. Engel, C. K., Kiema, T. R., Kalervo Hiltunen, J. and Wierenga, R. K. (1998) The crystal structure of enoyl-CoA hydratase complexed with octanoyl-CoA reveals the structural adaptations required for binding of a long chain fatty acid-CoA molecule. J. Mol. Biol. **275**, 847-859. doi:10.1006/jmbi.1997.1491

53. Kasaragod, P., Venkatesan, R., Kiema, T. R., Hiltunen, J. K. and Wierenga, R. K. (2010) Crystal structure of liganded rat peroxisomal multifunctional enzyme type 1: A flexible molecule with two interconnected active sites. J. Biol. Chem. **285**, 24089-24098. doi:10.1074/jbc.M110.117606

54. Kasaragod, P., Schmitz, W., Hiltunen, J. K. and Wierenga, R. K. (2013) The isomerase and hydratase reaction mechanism of the crotonase active site of the multifunctional enzyme (type-1), as deduced from structures of complexes with 3S-hydroxy-acyl-CoA. FEBS J. **280**, 3160-3175. doi:10.1111/febs.12150

55. Kim, J. -. P. and Miura, R. (2004) Acyl-CoA dehydrogenases and acyl-CoA oxidases: Structural basis for mechanistic similarities and differences. Eur. J. Biochem. **271**, 483-493. doi:10.1046/j.1432-1033.2003.03948.x

56. Cho, B. -., Knight, E. M. and Palsson, B. Ø. (2006) Transcriptional regulation of the fad regulon genes of escherichia coli by ArcA. Microbiology. **152**, 2207-2219. doi:10.1099/mic.0.28912-0

57. Liang, X., Le, W., Zhang, D. and Schulz, H. (2001) Impact of the intramitochondrial enzyme organization on fatty acid oxidation. Biochem. Soc. Trans. **29**, 279-282. doi:10.1042/bst0290279

Table 1. The apparent Michaelis-Menten constants for the ECH and HAD activities of EcTFE, anEcTFE and HsTFE with *2E*-butenoyl-CoA, *2E*-decenoyl-CoA and *2E*-hexadecenoyl-CoA. The used substrate concentrations range from 1 to 120 µM for 2E-butenoyl-CoA and 2E-decenoyl-CoA and from 0.5 to 45 µM for 2*E*-hexadecenoyl-CoA.

kinetic parameters	**EcTFE**		**anEcTFE**		**HsTFE**	
	ECH	**HAD**	**ECH**	**HAD**	**ECH**	**HAD**
with *2E*-butenoyl-CoA						
k_{cat} (s^{-1})	383.9 ± 88.1	7.5 ± 1.4	-	-	-	-
K_m (µM)	33.8 ± 9.6	25.3 ± 4.1	-	-	-	-
k_{cat}/K_m (M^{-1} s^{-1})	$11.5x10^6$ ± $0.6x10^6$	$0.3x10^6$ ± $0.05x10^6$	-	-	-	-
with *2E*-decenoyl-CoA						
k_{cat} (s^{-1})	8.1 ± 1.2	1.6 ± 0.2	192.5 ± 35	5.4 ± 0.5	83.2 ± 10.1	5.7 ± 0.7
K_m (µM)	5.6 ± 1.6	6.7 ± 0.2	30.7 ± 10.9	3.4 ± 0.6	5.7 ± 0.8	1.3 ± 0.1
k_{cat}/K_m (M^{-1} s^{-1})	$1.5x10^6$ ± $0.2x10^6$	$0.3x10^6$ ± $0.07x10^6$	$6.6x10^6$ ± $1.2x10^6$	$1.6x10^6$ ± $0.4x10^6$	$14.8x10^6$ ± $1.45x10^6$	$4.37x10^6$ ± $0.74x10^6$
with *2E*-hexadecenoyl-CoA						
k_{cat} (s^{-1})	3.6 ± 0.9	2.1 ± 0.7	23.8 ± 1.9	5.8 ± 0.7	52.2 ± 2.2	2.5 ± 0.3
K_m (µM)	7.3 ± 1.2	1.6 ± 0.4	2.5 ± 0.4	1.0 ± 0.2	11.5 ± 2.4	0.9 ± 0.2
k_{cat}/K_m (M^{-1} s^{-1})	$0.5x10^6$ ± $0.1x10^6$	$1.3x10^6$ ± $0.3x10^6$	$9.6x10^6$ ± $1.7x10^6$	$5.8x10^6$ ± $1.3x10^6$	$4.7x10^6$ ± $1.1x10^6$	$2.8x10^6$ ± $0.4x10^6$

- : not measurable

Table 2. SAXS analysis for EcTFE and anEcTFE.

Parameters	**EcTFE**	**anEcTFE**
Beamline	B21, DLS, UK	BM29, ESRF, France
I(0) cm^{-1}	0.065	0.464
R_g (Å)	45.96	61.54
Dmax (Å)	160.35	195.69
Porod volume, Po ($Å^{-3}$)	503163	944857
Molecular mass derived from MM_{Qp} MoW, V_c, and Size&Shape method (kDa)	266, 271, - , 248	573, - , - , 521
χ^2 (goodness of fit) with the atomic model (FoXS, CRYSOL)	2.74, 1.35	3.50, 3.50
SASBDB accession code	SASDEL9	SASDEM9

- **: not applicable**

Figure legends

Figure 1. Schematic presentation of the fatty acid β-oxidation pathways in *E. coli* (aerobic and anaerobic) and mitochondria (soluble and membrane bound). The gene names are given in italics. The membrane bound enzymes are highlighted in boxes (when membrane association is known). The main products of these pathways are reducing equivalents (electrons) and acetyl-CoA. The reducing equivalents are further processed by auxiliary proteins that link the β-oxidation pathway to the respiratory chain, whereas acetyl-CoA is further metabolized by the TCA cycle.

Figure 2. Purification and characterization of EcTFE, anEcTFE and HsTFE. **a.** SEC profile of EcTFE (red) anEcTFE (green) and HsTFE (cyan), using a Superdex 200 Hiload 16/60 column. All three complexes consist of α and β subunits as shown by cropped SDS-PAGE, where M indicates lane for standard protein marker: the 70 kDa and the 40 kDa markers are indicated. The complete SDS-PAGE gels with molecular size for each marker bands are presented in Supplementary Figure 3a-b. **b.** CD spectrum of EcTFE (red), anEcTFE (green) and HsTFE (cyan). **c.** SEC profile of anEcTFE purified in the absence and in the presence of various detergents. **d.** SEC profile of HsTFE purified in the presence of various detergents. **e.** TFE-α overall activities (HAD activity, measured at 340 nm) of anEcTFE and HsTFE solubilized in various detergents using 60 µM *2E*-decenoyl-CoA as the substrate. **f.** Cropped Blue Native-PAGE of anEcTFE and HsTFE purified in the presence of different detergents. M, BSA (133 kDa and 66 kDa) and MtTFE (240 kDa) identify lanes with marker proteins. The complete BN-PAGE gels with molecular size for each marker bands are shown in Supplementary Figure 3c-e.

Figure 3. Substrate preferences. **a.** The covalent structures of the various substrates used for measuring the specific activities of EcTFE, anEcTFE and HsTFE. **b**. Specific activities of the ECH and HAD active sites of EcTFE, anECTFE and HsTFE at 60 µM substrate concentration.

Figure 4. SAXS data analysis of EcTFE **a.** Kratky plot of EcTFE suggesting the protein is in a folded state in solution. **b.** Pairwise distance distribution curve of EcTFE with a D_{max} of 160 Å. **c.** The experimental EcTFE SAXS scattering curve fitted with the EcTFE atomic model using the FoXS server (χ^2 = 2.74). **d.** The SAXS *ab initio* shape of EcTFE superimposed with the EcTFE atomic model using the program SUPCOMB. **e.** The electron density sliced map of EcTFE generated from experimental SAXS scattering by the DENSSWeb server fitted with the EcTFE atomic model. The density map is shown at contour levels 3, 5 and 8 sigmas in green, yellow and red surfaces respectively.

Figure 5. SAXS data analysis of anEcTFE. **5a.** Kratky plot for anEcTFE. **5b.** Pair distance distribution curve for anEcTFE with D_{max} value about 196Å. **5c.** The experimental anEcTFE SAXS scattering curve fitted with the anEcTFE heterotetramer (green line; χ^2 = 174), the anEcTFE heterooctamer, being similar to HsTFE octameric assembly (blue line; χ^2 = 52) and the anEcTFE heterooctamer, being the proposed model (red line; χ^2 = 3.50). **5d.** SAXS *ab initio* shape of anEcTFE superimposed with the proposed anEcTFE heterooctameric model. **5e.** Sliced electron density map of anEcTFE generated from experimental SAXS by the DENSSWeb server is fitted with the anEcTFE heterooctameric model. The density map is shown at contour levels 3, 5 and 8 sigmas in green, yellow and red surfaces, respectively.

Figure 6. Negative staining EM analysis of EcTFE and anEcTFE. **6a.** Representative micrograph showing negatively stained EcTFE particles on the grid. **6b.** 2D classes of EcTFE particles processed by RELION software. **6c.** the 3D- EM map of EcTFE superimposed with EcTFE model based on the PfTFE assembly. **6d.** a representative 1D micrograph showing negatively stained anEcTFE particles on the grid. **6e.** 2D classes of anEcTFE particles. **6f.** the 3D- EM map of anEcTFE superimposed with the proposed anEcTFE heterooctameric model based on the HsTFE tetramer assembly. The maps shown in Figures 6c and 6f are not on the same scale.

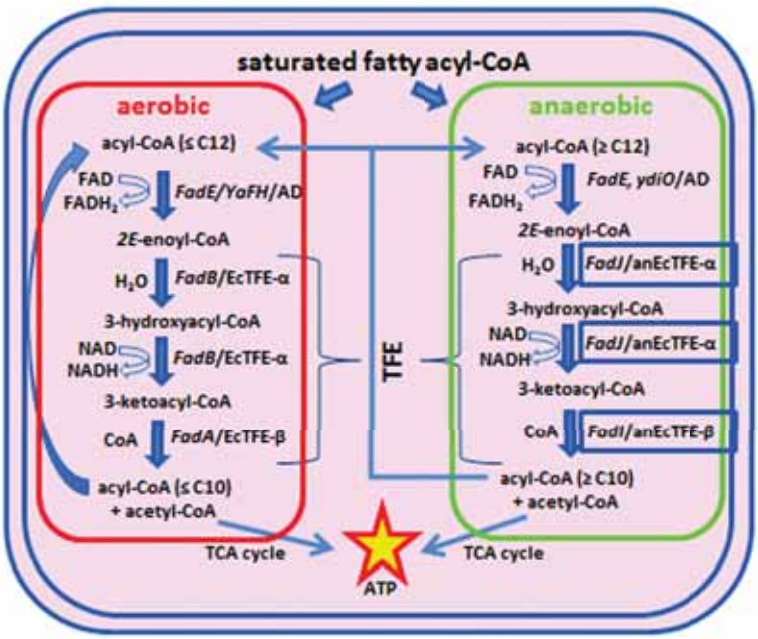

E. coli

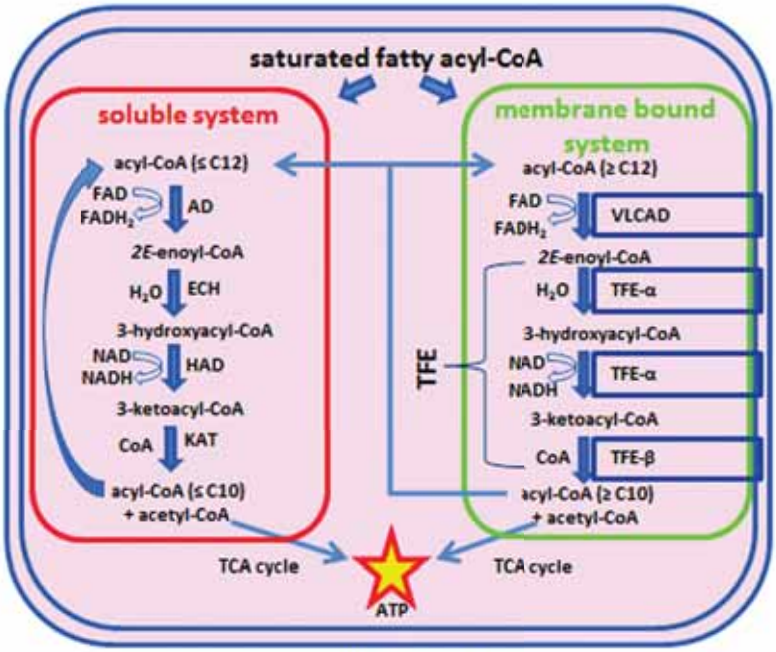

mitochondria

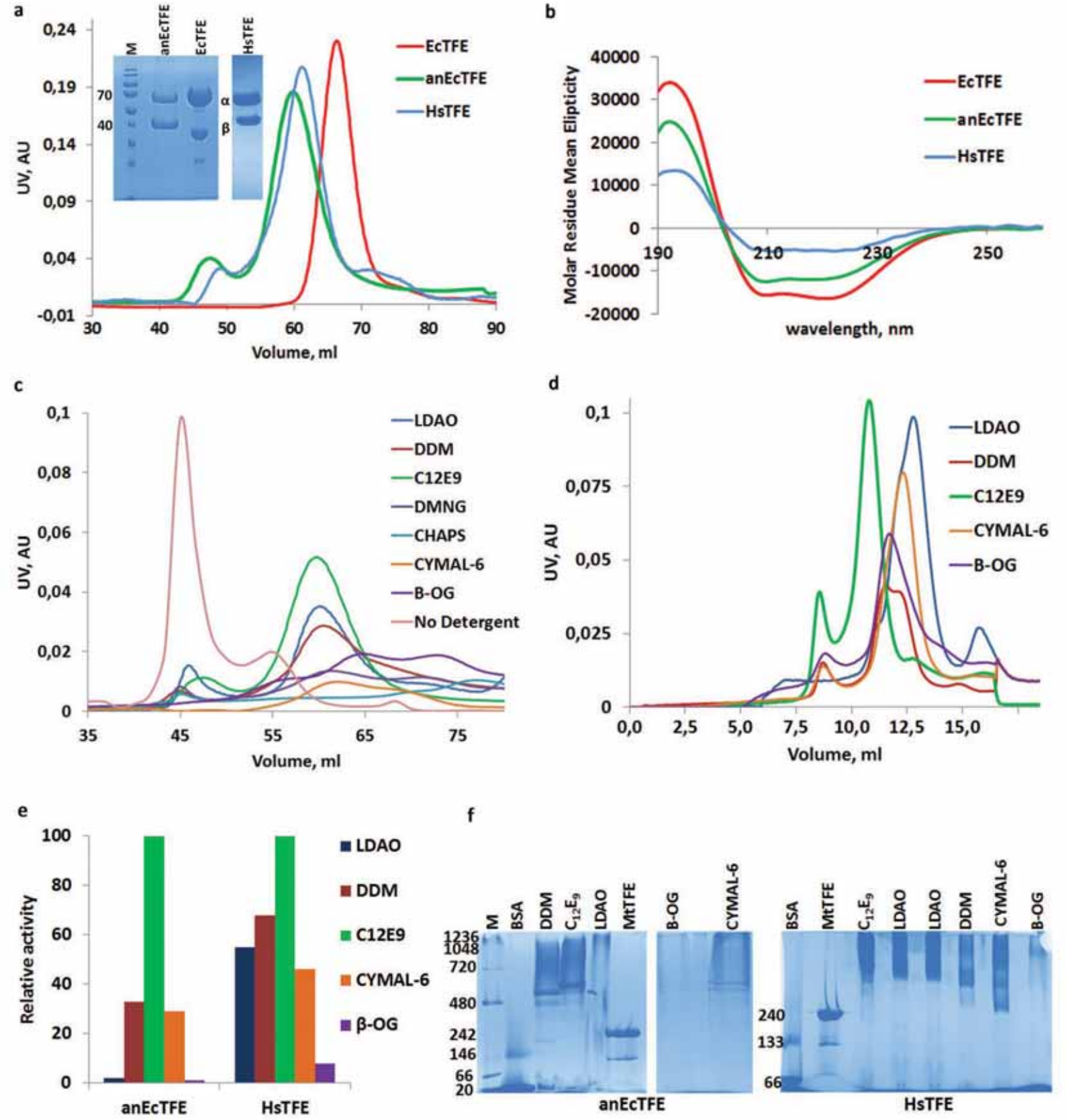
a
UV, AU
Volume, ml
EcTFE
anEcTFE
HsTFE
M
anEcTFE
EcTFE
HsTFE
70
40
α
β
b
Molar Residue Mean Elipticity
wavelength, nm
EcTFE
anEcTFE
HsTFE
c
UV, AU
Volume, ml
LDAO
DDM
C12E9
DMNG
CHAPS
CYMAL-6
B-OG
No Detergent
d
UV, AU
Volume, ml
LDAO
DDM
C12E9
CYMAL-6
B-OG
e
Relative activity
LDAO
DDM
C12E9
CYMAL-6
β-OG
anEcTFE
HsTFE
f
M
BSA
DDM
C12E9
LDAO
MtTFE
B-OG
CYMAL-6
1236
1048
720
480
242
146
66
20
anEcTFE
BSA
MtTFE
C12E9
LDAO
LDAO
DDM
CYMAL-6
B-OG
240
133
66
HsTFE

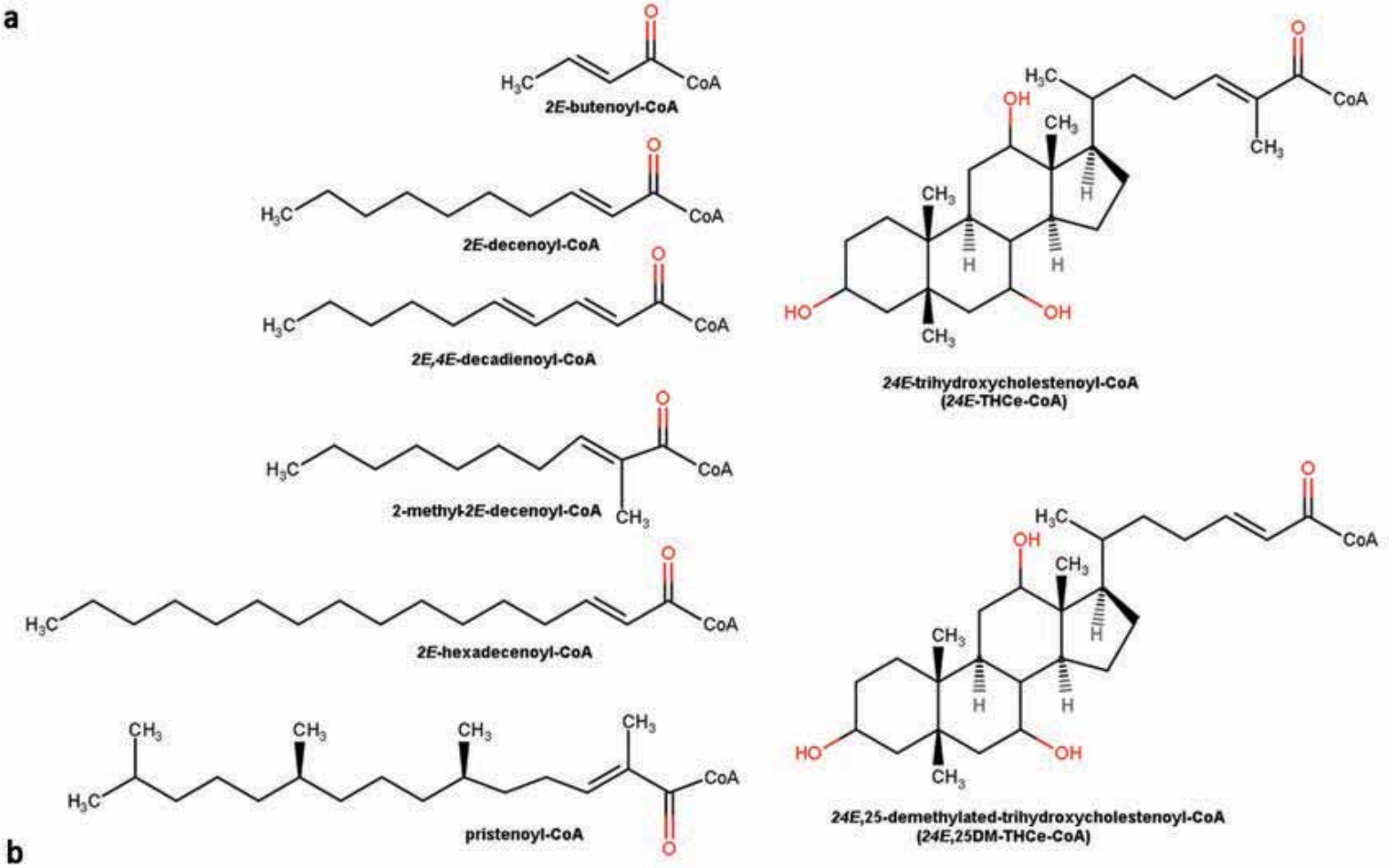
a
2E-butenoyl-CoA
2E-decenoyl-CoA
2E,4E-decadienoyl-CoA
2-methyl-2E-decenoyl-CoA
2E-hexadecenoyl-CoA
pristenoyl-CoA
24E-trihydroxycholestenoyl-CoA
(24E-THCe-CoA)
24E,25-demethylated-trihydroxycholestenoyl-CoA
(24E,25DM-THCe-CoA)

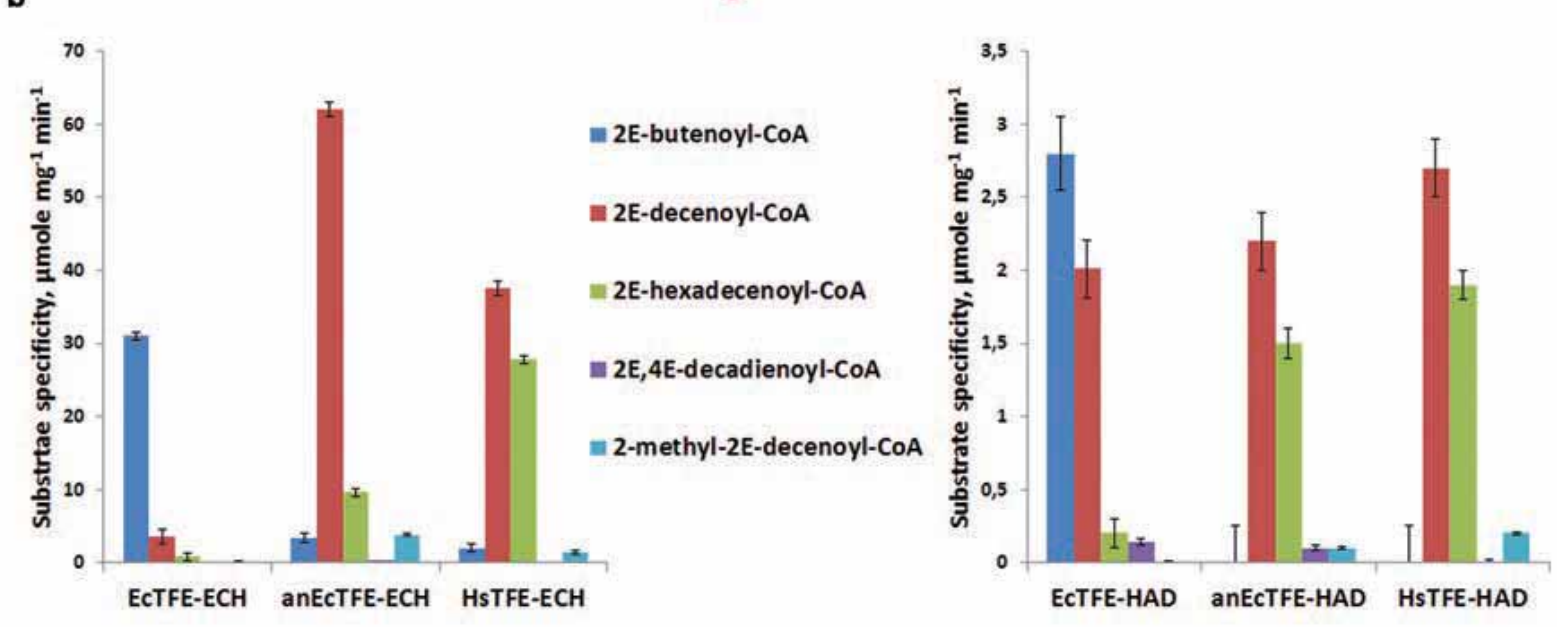
b
Substrtae specificity, µmole mg-1 min-1
2E-butenoyl-CoA
2E-decenoyl-CoA
2E-hexadecenoyl-CoA
2E,4E-decadienoyl-CoA
2-methyl-2E-decenoyl-CoA
EcTFE-ECH
anEcTFE-ECH
HsTFE-ECH
Substrate specificity, µmole mg-1 min-1
EcTFE-HAD
anEcTFE-HAD
HsTFE-HAD

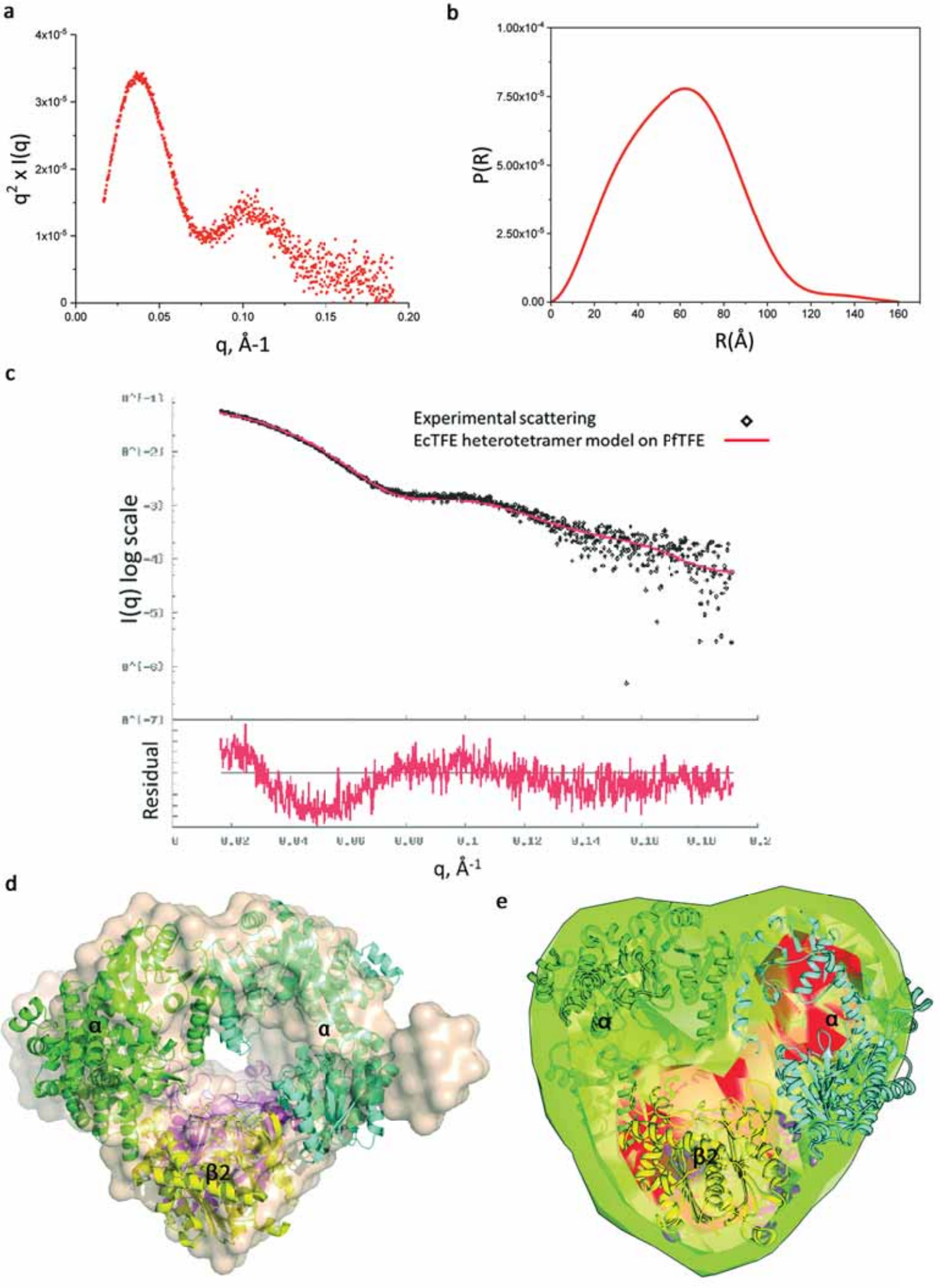
a
4x10-5
3x10-5
2x10-5
1x10-5
0
q2 x I(q)
0.00
0.05
0.10
0.15
0.20
q, Å-1
b
1.00x10-4
7.50x10-5
5.00x10-5
2.50x10-5
0.00
P(R)
0
20
40
60
80
100
120
140
160
R(Å)
c
Experimental scattering
EcTFE heterotetramer model on PfTFE
I(q) log scale
Residual
q, Å-1
d
α
α
β2
e
α
α
β2

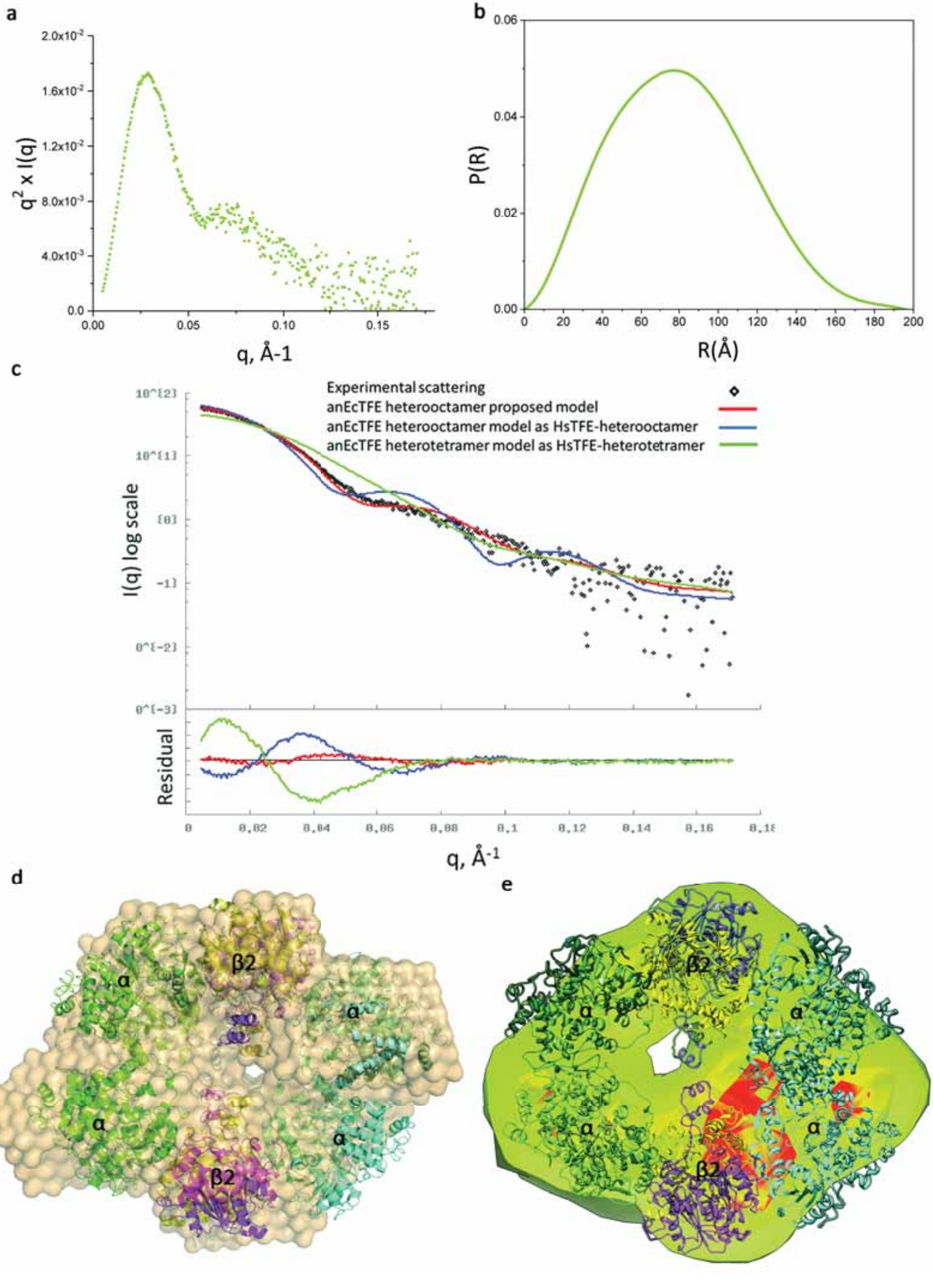
a
2.0x10-2
1.6x10-2
1.2x10-2
8.0x10-3
4.0x10-3
0.0
q2 x I(q)
0.00
0.05
0.10
0.15
q, Å-1
b
0.06
0.04
0.02
0.00
P(R)
0
20
40
60
80
100
120
140
160
180
200
R(Å)
c
Experimental scattering
anEcTFE heterooctamer proposed model
anEcTFE heterooctamer model as HsTFE-heterooctamer
anEcTFE heterotetramer model as HsTFE-heterotetramer
I(q) log scale
Residual
0.02
0.04
0.06
0.08
0.1
0.12
0.14
0.16
q, Å-1
d
α
β2
α
α
α
β2
e
α
β2
α
α
α
β2

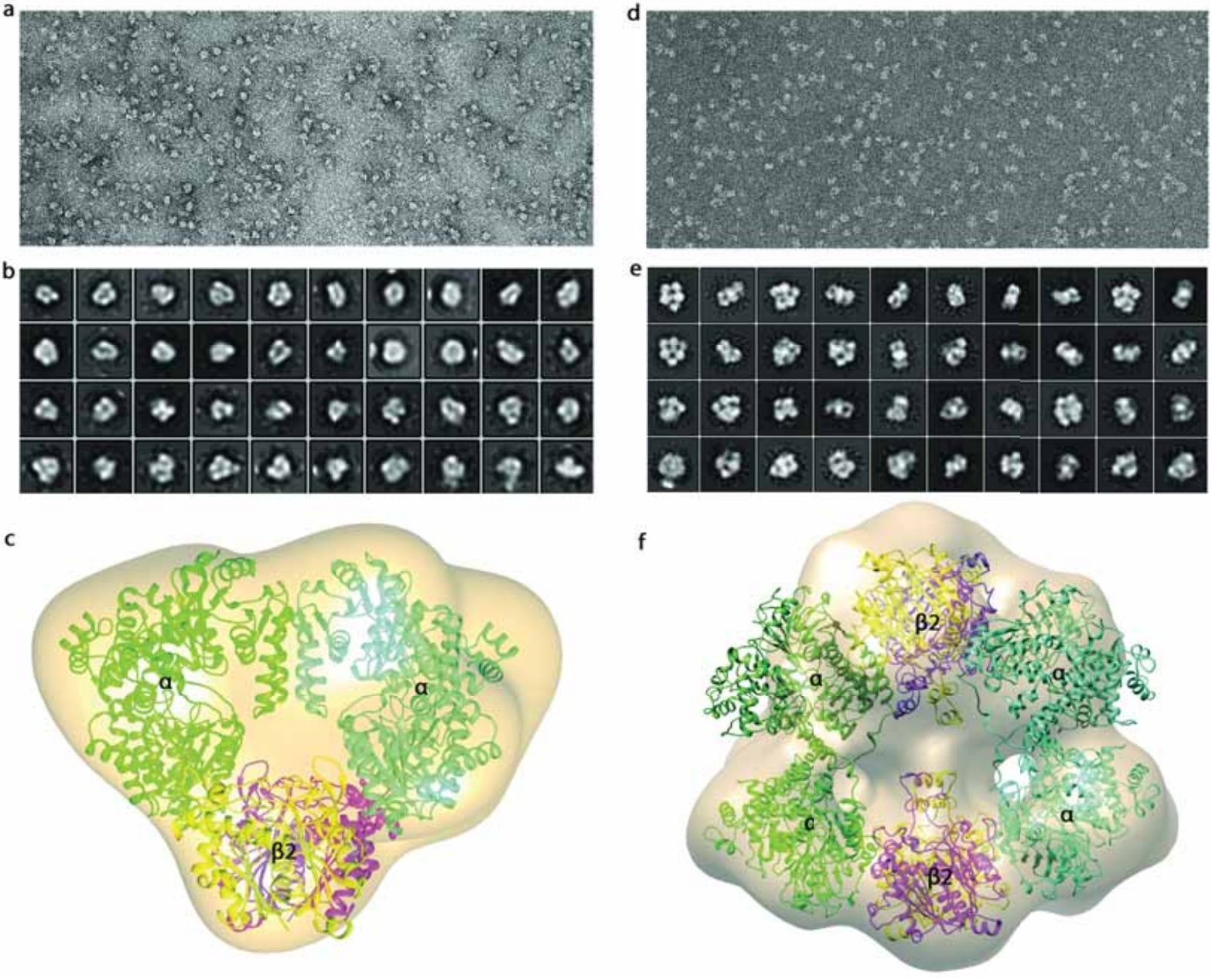
a
b
c
α
α
β2
d
e
f
β2
α
α
α
α
β2

Supplementary Information

Complementary substrate specificity and distinct quaternary assembly of the *Escherichia coli* aerobic and anaerobic beta-oxidation trifunctional enzyme complexes

Shiv K. Sah-Teli[1], Mikko J. Hynönen[1], Werner Schmitz[2], James A. Geraets[3,4], Jani Seitsonen[3], Jan Skov Pedersen[5], Sarah J. Butcher[3], Rik K. Wierenga[1] and Rajaram Venkatesan[1*]

[1]Faculty of Biochemistry and Molecular Medicine, and Biocenter Oulu, University of Oulu, Finland

[2]Theodor-Boveri-Institut für Biowissenschaften der Universität Würzburg, Germany

[3]Helsinki Institute of Life Science, University of Helsinki, Finland

[4]Forschungszentrum Jülich, Jülich, Germany

[5]Department of Chemistry and Interdisciplinary Nanoscience Center (iNANO), Aarhus University, Denmark

*rajaram.venkatesan@oulu.fi

Supplementary Table 1. List of primers used in this study.

Primers for EcTFE (His-α/β) construct	
FadB-F	5’ CATCACCACAGCCAGGATCCGATGCTTTACAAAGGCGAC 3’
FadB-R	5’ TTATGCGGCCGCAAGCTTTTAAGCCGTTTTCAGGTC 3’
FadA-F	5’ GAAGGAGATATACATATGATGGAACAGGTTGTCATTGTC 3’
FadA-R	5’ ACCAGACTCGAGGGTACCTTAAACCCGCTCAAACAC 3’
Primers for anEcTFE (His-α/β) construct	
Fad J-F	5’GGGCAGCAGCCATCACCATCATCACCACAGCCAGGATCCGATGGAAATGACATCAGCGTTTACCC 3’
Fad J- R	5’GCATTATGCGGCCGCAAGCTTTTATTGCAGGTCAGTTGCAGTTGTTTTCC 3’
FadI-F	5’GGAGATATACATATGATGGGTCAGGTTTTACCGCTGGTTACCCGC 3’
FadI-R	5’GCGGTTTCTTTACCAGACTCGAGTTATTCCGCCTCCAGAACCATTGCCGCGCC 3’
Primers for anEcTFE (α/His-β) construct	
D2-FadI-F	5’GGGCAGCAGCCATCACCATCATCACCACAGCCAGGATCCGATGGGTCAGGTTTTACCGCTGGTTACCCGC 3’
D2-FadI-R	5’GCATTATGCGGCCGCAAGCTTTTATTCCGCCTCCAGAACCATTGCCGCGCC 3’
D2-FadJ-F	5’GTATAAGAAGGAGATATACATATGATGGAAATGACATCAGCGTTTACCC 3’
D2-FADJ-R	5’GCGGTTTCTTTACCAGACTCGAGTTATTGCAGGTCAGTTGCAGTTGTTTTCC 3’
Primers for HsTFE (α/His-β) construct	
HADHA-F	5’ATTAGTTAAGTATAAGAAGGAGATATACATATGACCAGAACCCATATTAACTATGG 3’
HADHA-R	5’CAGCAGCGGTTTCTTTACCAGACTCGAGTCACTGGTAGAACTTCTTGTTA 3’
HADHB-F	5’AGCCATCACCATCATCACCACAGCCAGGCTGCCCCAGCTGTCCAGACC 3’
HADHB-R	5’ AGCATTATGCGGCCGCAAGCTTGTCGACTTATTTTGGATAAGCTTCCACT 3’

Supplementary Table 2. Parameters used for SAXS data collection and analysis for EcTFE and anEcTFE.

Parameters	**EcTFE**	**anEcTFE**
SEC-SAXS column	Shodex KW403	Superdex 200 5/150 GL, GE Healthcare
Loading concentration (mg mL^{-1})	6.2	3.5
Injected volume (µL)	30	30
Flowrate (mL min^{-1})	0.16	0.15
Solvent (buffer)	20 mM HEPES, 120 mM KCl, 2.5 mM DTT, pH 7.2	50 mM Tris, 500 mM NaCl, 5% glycerol, 0.05% $C_{12}E_9$, 2.5 mM DTT at pH 8.0
Beamline	B21, DLS, UK	BM29, ESRF, France
Beam size (µm)	250x250	50x50
Detector	Pilatus 2M	Pilatus 1M
Wavelength (Å)	1	1
Camera length (m)	4.014	2.867
q measurement range ($Å^{-1}$)	0.0031 to 0.38	0.0025 to 0.5
Exposure time (s)	3	1
Sample configuration	SEC-SAXS with quartz cell capillary	SEC-SAXS with quartz cell capillary
Sample temperateure (ºC)	20	20
SAXS data reduction	I(q) vs q, solvent subtraction using Scatter	I(q) vs q, solvent subtraction using Scatter
Extinction coefficient estimate	Protparam	Protparam
Basic analysis: Guiner, p(r)	PRIMUS from ATSAS, SCATTER	PRIMUS from ATSAS, SCATTER
Shape /bead modelling	DAMMIN ATSAS online	DAMMIN ATSAS online

Atomic structure modelling	SWISS-MODEL, COOT, FoXS, CRYSOL	SWISS-MODEL, COOT, FoXS, CRYSOL
Three-dimensional graphic model-representations	PyMOL	PyMOL
guinier and *P(r)* analysis		
I(0) cm^{-1}	0.065	0.464
q range ($Å^{-1}$)	0.0167- 0.1732	0.0050- 0.1290
R_g (Å)	45.96	61.54
qR_g max	1.29	1.27
Dmax (Å)	160.35	195.69
χ^2 (total estimate from GNOM)	0.8961	0.7262
Porod volume, Po ($Å^{-3}$)	503163	944857
Molecular mass derived from MM_{Qp}, MoW, V_c, and Size&Shape method (kDa)	266, 271, - , 248	573, - , - , 521
DAMMIN		
q range for fitting ($Å^{-1}$)	0.0167- 0.1732	0.0050- 0.1290
Symmetry, anisotropy assumption	P1, unknown	P1, unknown
χ^2 (goodness of fit)	1.03	1.01
Atomistic modeling		
Crystal structures	PfTFE structure (PDB code: 1WDM) as reference structure	HsTFE structure (PDB code: 5ZQZ) as reference structure for the tetrameric assembly
Atomic model used	EcTFE heterotetramer model on PfTFE	anEcTFE heterooctamer proposed model (based on HsTFE heterotetramer assembly)

q range for all modelling	0.0167- 0.19	0.0050- 0.17
FoXS		
χ^2 (goodness of fit) with the atomic model	2.74	3.50
Predicted Rg (Å)	42.2	59.1
c1, c2	1.05, 1.26	0.99, 0.45
CRYSOL		
χ^2 (goodness of fit) with the atomic model	1.35	3.50
Predicted Rg (Å)	44.27	59.64
SASBDB accession code	SASDEL9	SASDEM9

- **: not applicable**

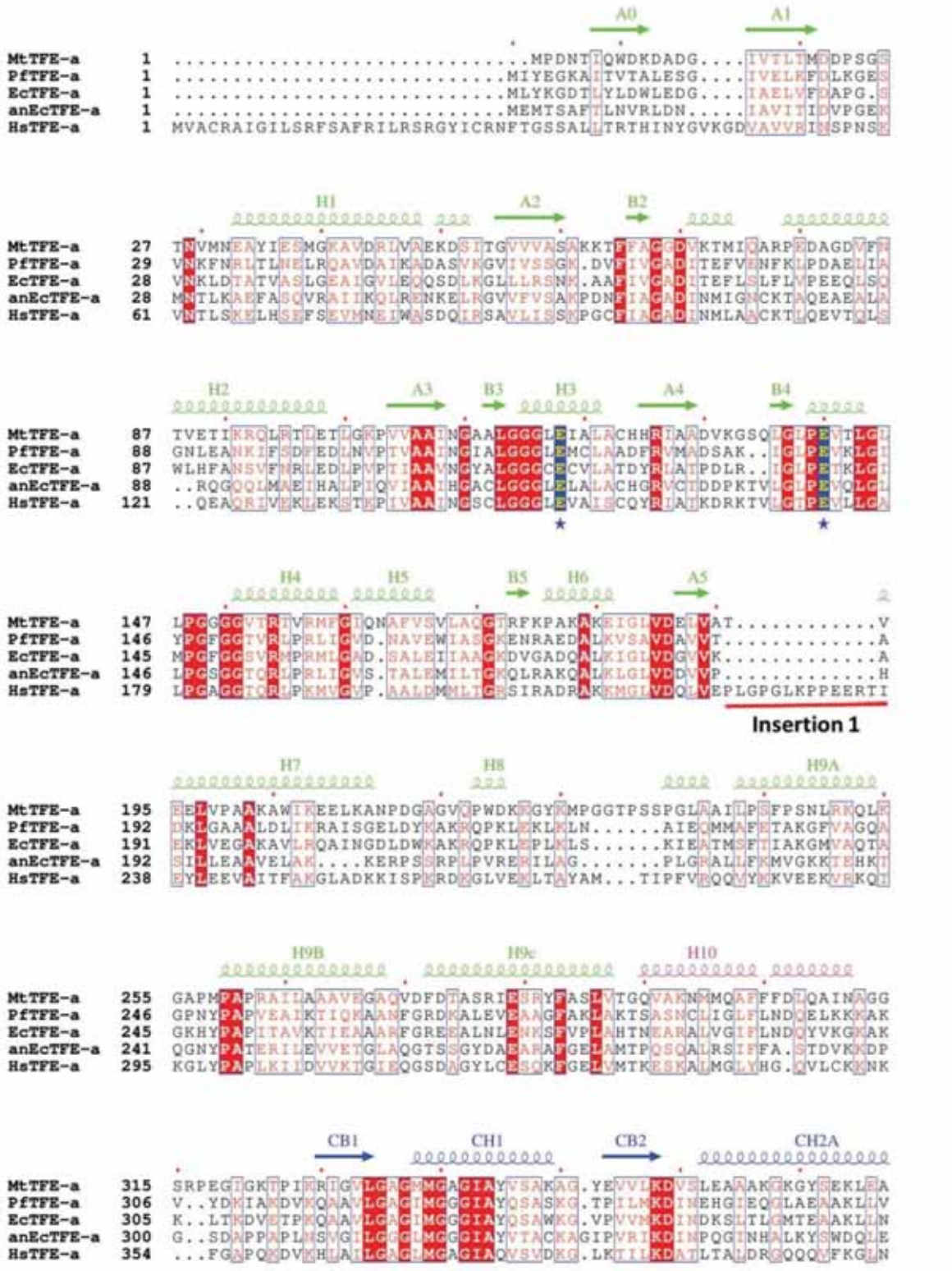
A0
A1
MtTFE-a 1
PfTFE-a 1
EcTFE-a 1
anEcTFE-a 1
HsTFE-a 1
H1
A2
B2
MtTFE-a 27
PfTFE-a 29
EcTFE-a 28
anEcTFE-a 28
HsTFE-a 61
H2
A3
B3
H3
A4
B4
MtTFE-a 87
PfTFE-a 88
EcTFE-a 87
anEcTFE-a 88
HsTFE-a 121
H4
H5
B5
H6
A5
MtTFE-a 147
PfTFE-a 146
EcTFE-a 145
anEcTFE-a 146
HsTFE-a 179
Insertion 1
H7
H8
H9A
MtTFE-a 195
PfTFE-a 192
EcTFE-a 191
anEcTFE-a 192
HsTFE-a 238
H9B
H9c
H10
MtTFE-a 255
PfTFE-a 246
EcTFE-a 245
anEcTFE-a 241
HsTFE-a 295
CB1
CH1
CB2
CH2A
MtTFE-a 315
PfTFE-a 306
EcTFE-a 305
anEcTFE-a 300
HsTFE-a 354

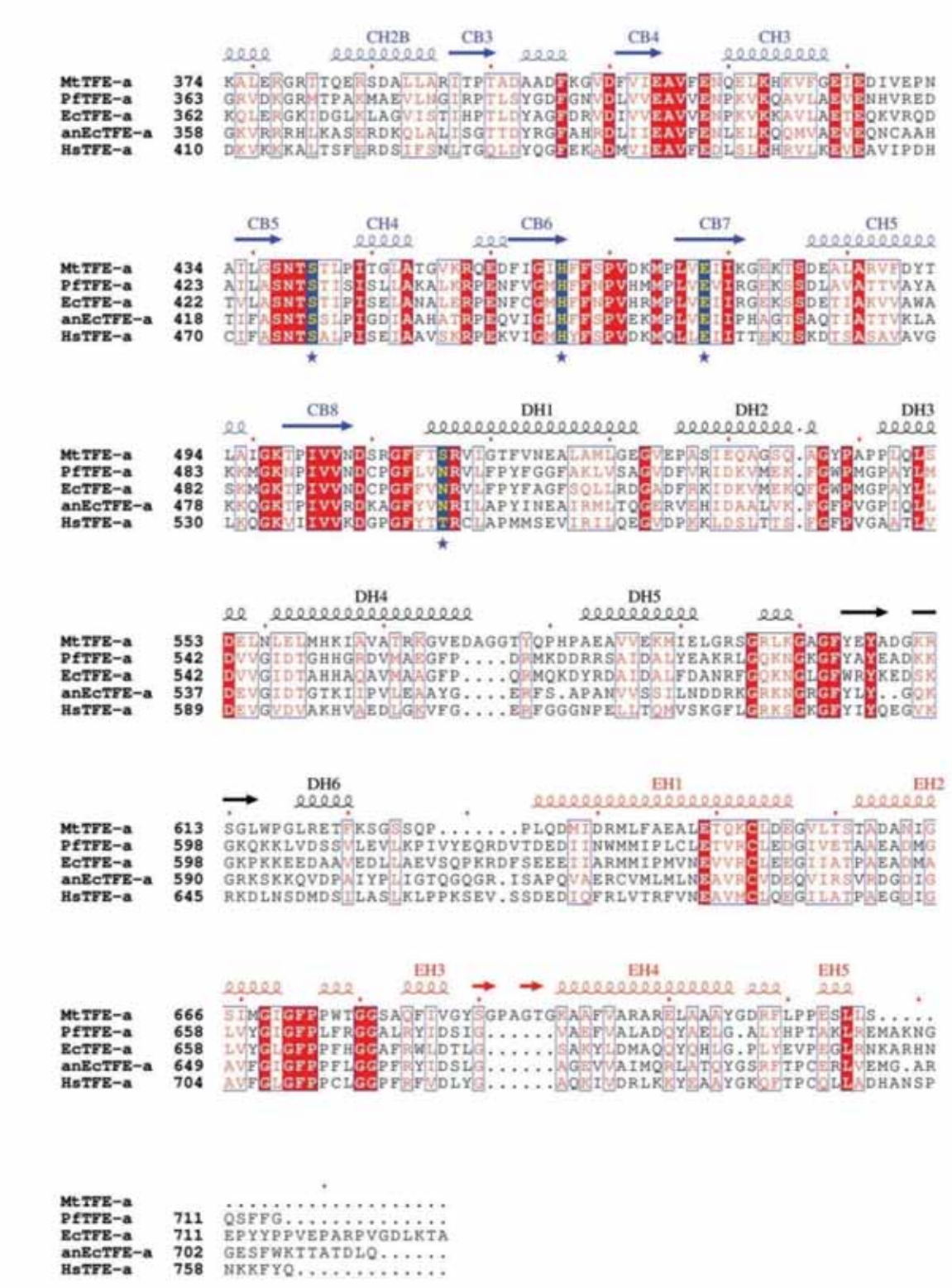

Supplementary Figure 1. Multiple sequence alignment of TFE-α from different organisms. The secondary structure elements are from the structure of the α chain of *Mycobacterium tuberculosis* TFE (identified as MtTFE-a) (PDB code: 4B3H). The active site residues in the hydratase and dehydrogenase domains are indicated with blue blocks with yellow residue names and blue stars at the bottom. The unique insertion in HsTFE-α is identified with a red line below the sequence. Every tenth residue of anEcTFE-α is marked with a red dot above the sequences.

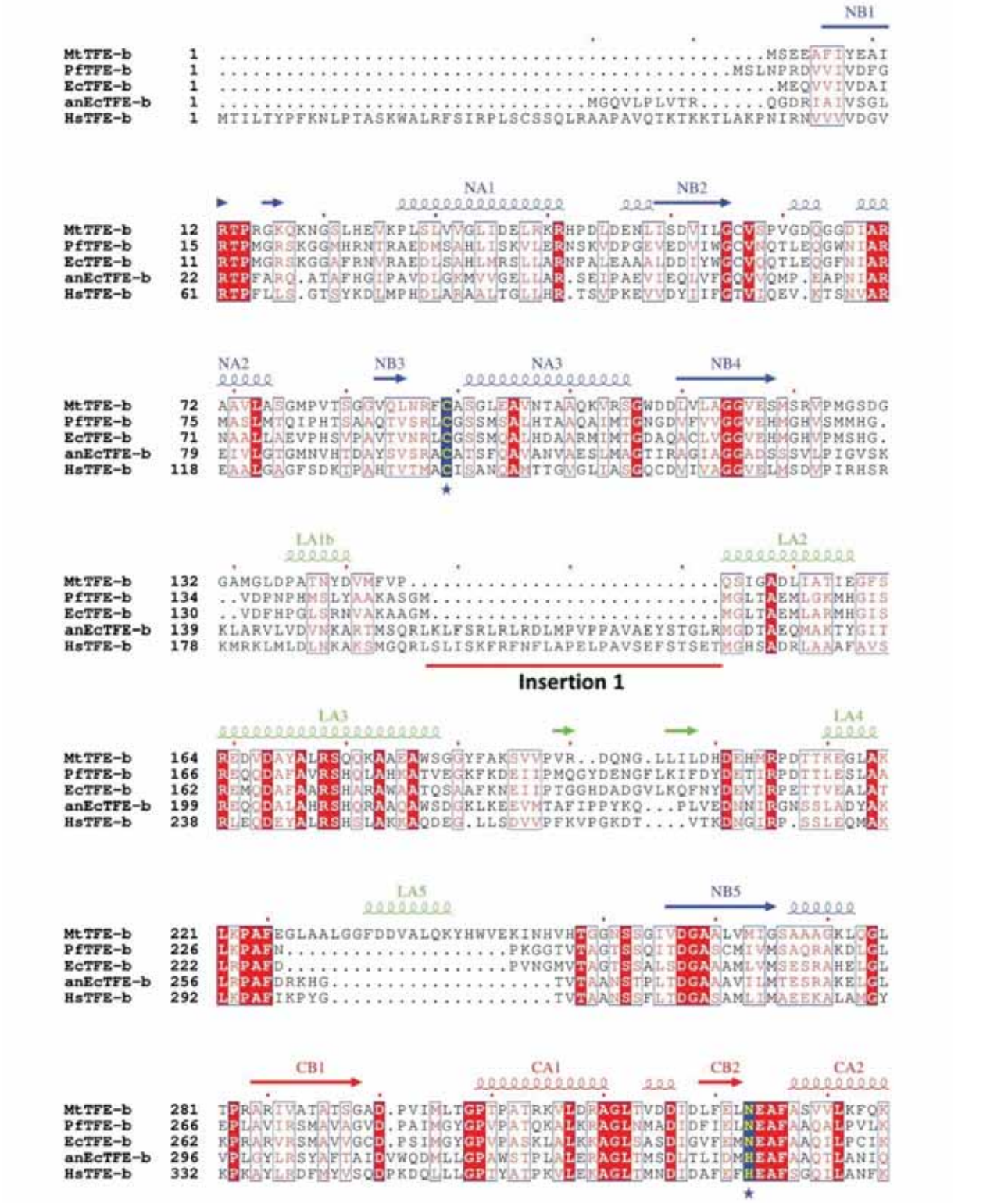
NB1
MtTFE-b 1 .....MSEEAFIYEAI
PfTFE-b 1 .....MSLNPRDVVIVDFG
EcTFE-b 1 .....MEQVVIVDAI
anEcTFE-b 1 .....MGQVLPLVTR.....QGDRIAIVSGL
HsTFE-b 1 MTILTYPFKNLPTASKWALRFSIRPLSCSSQLRAAPAVQTKTKKTLAKPNIRNVVVVDGV
NA1
NB2
MtTFE-b 12 RTPRGKQKNGSLHEVKPLSLVVGLIDELRKPHPDLDENLISDVILGCVSPVGDQGGDIAR
PfTFE-b 15 RTPMGRSKGGMHRNTRAEDMSAHLISKVLERNSKVDPGEVEDVIWGCVNQTLEQGWNIAR
EcTFE-b 11 RTPMGRSKGGAFRNVRAEDLSAHLMRSLLARNPALEAAALDDIYWGCVQQTLEQGFNIAR
anEcTFE-b 22 RTPFARQ.ATAFHGIPAVDLGKMVVGELLAR.SEIPAEVIEQLVFGQVVQMP.EAPNIAR
HsTFE-b 61 RTPFLLS.GTSYKDLMPHDLARAALTGLLHR.TSVPKEVVDYIIFGTVLQEV.KTSNVAR
NA2
NB3
NA3
NB4
MtTFE-b 72 AAVLASGMPVTSGGVQLNRFGASGLEAVNTAAQKVRSGWDDLVLAGGVESMSRVPMGSDG
PfTFE-b 75 MASLMTQIPHTSAAQTVSRLGGSSMSALHTAAQAIMIGNGDVFVVGGVEHMGHVSMMHG.
EcTFE-b 71 NAALLAEVPHSVPAVTVNRLGGSSMQALHDAARMIMIGDAQACLVGGVEHMGHVPMSHG.
anEcTFE-b 79 EIVLGTGMNVHTDAYSVSRAGATSFQAVANVAESLMAGTIRAGIAGGADSSSVLPIGVSK
HsTFE-b 118 EAALGAGFSDKTPAHTVTMAGISANQANTTGVGLIASGQCDVIVAGGVELMSDVPIRHSR
LA1b
LA2
MtTFE-b 132 GAMGLDPATNYDVMFVP.....QSIGADLIATIEGFS
PfTFE-b 134 ..VDPNPHMSLYAAKASGM.....MGLTAEMLGKMHGIS
EcTFE-b 130 ..VDFHPGLSRNVAKAAGM.....MGLTAEMLARMHGIS
anEcTFE-b 139 KLARVLVDVNKARTMSQRLKLFSRLRLRDLMPVPPAVAEYSTGLRMGDTAEQMAKTYGIT
HsTFE-b 178 KMRKLMLDLHKAKSMGQRLSLISKFRFNFLAPELPAVSEFSTSETMGHSADRLAAAFAVS
Insertion 1
LA3
LA4
MtTFE-b 164 REDVDAYALRSQQKAAEAWSGGYFAKSVVPVR..DQNG.LLILDHDEHMRPDTTKEGLAK
PfTFE-b 166 REQQDAFAVRSHQLAHKATVEGKFKDEIIPMQGYDENGFLKIFDYDETIRPDTTLESLAA
EcTFE-b 162 REMQDAFAARSHARAWAATQSAAFKNEIIPTGGHDADGVLKQFNYDEVIRPETTVEALAT
anEcTFE-b 199 REQQDALALHRSHQRAAQAWSDGKLKEEVMTAFIPPYKQ...PLVEDNNIRGNSSLADYAK
HsTFE-b 238 RLEQDEYALRSHSLAKKAQDEG.LLSDVVPFKVPGKDT....VTKDNGIRP.SSLEQMAK
LA5
NB5
MtTFE-b 221 LKPAFEGLAALGGFDDVALQKYHWVEKINHVHTGGNSSGIVDGAALVMIGSAAAGKLCGL
PfTFE-b 226 LKPAFN.....PKGGTVTAGTSSQITDGASCMIVMSAQRAKDLGL
EcTFE-b 222 LKPAFD.....PVNGMVTAGTSSALSDGAAAMLVMSESRAHELGL
anEcTFE-b 256 LKPAFDRKHG.....TVTAANSTPLTDGAAAVILMTESRAKELGL
HsTFE-b 292 LKPAFIKPYG.....TVTAANSSFLTDGASAMLIMAEEKALAMGY
CB1
CA1
CB2
CA2
MtTFE-b 281 TPRARIVATATSGAD.PVIMLTGPTPATRKVLDRAGLTVDDIDLFELNEAFASVVLKFQK
PfTFE-b 266 EPLAVIRSMAVAGVD.PAIMGYGPVPATQKALKRAGLNMADIDFIELNEAFAAQALPVLK
EcTFE-b 262 KPRARVRSMAVVGCD.PSIMGYGPVPASKLALKRAGLSASDIGVFEMNEAFAAQILPCIK
anEcTFE-b 296 VPLGYLRSYAFTAIDVWQDMLLGPAWSTPLALERAGLTMSDLTLIDMHEAFAAQTLANIQ
HsTFE-b 332 KPKAYLHDFMYVSQDPKDQLLLGPTYATPKVLENAGLTMNDIDAFEFHEAFSGQILANFK

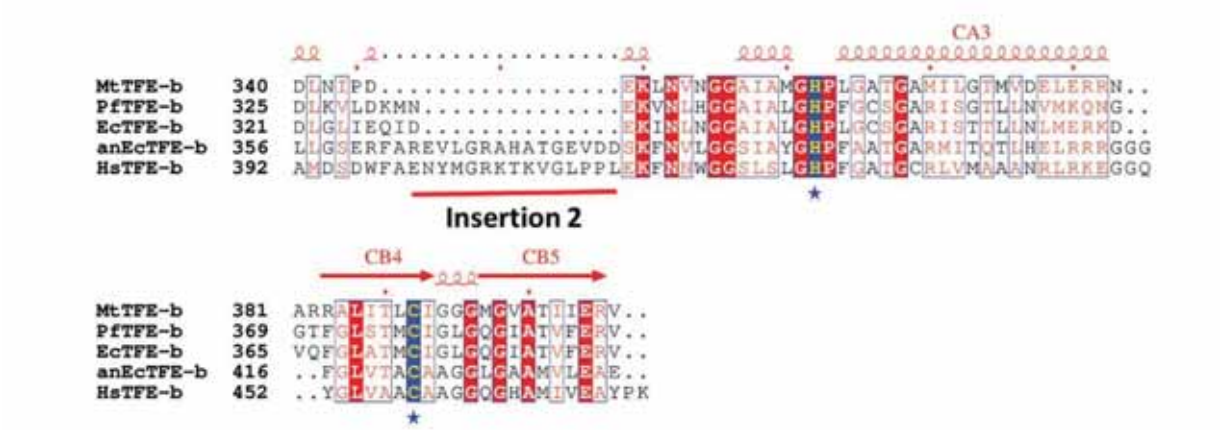

Supplementary Figure 2. Multiple sequence alignment of TFE-β from different organisms. The secondary structure elements are from the structure of the *M. tuberculosis* TFE-β chain (identified as MtTFE-b) (PDB code: 4B3H). The active site residues are indicated with blue blocks with yellow residue names and blue stars at the bottom. The unique insertions in HsTFE-β and anEcTFE-β are identified with red lines below the sequence. Every tenth residue of anEcTFE-β is marked with a red dot above the sequences.

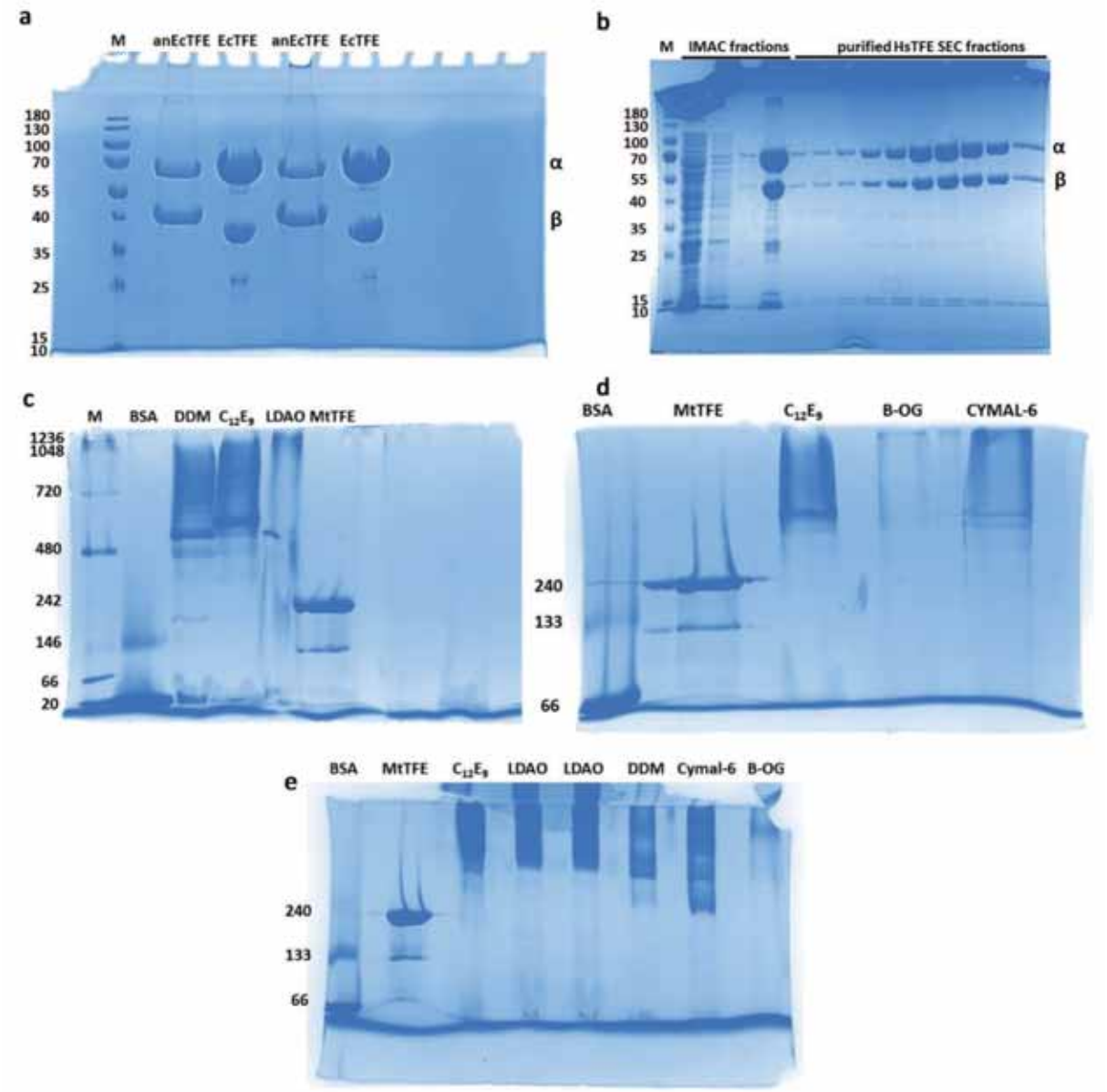

Supplementary Figure 3. Complete PAGE gel images. The molecular size for each marker bands are marked on the left side of each gel. **a.** SDS-PAGE of purified anEcTFE and EcTFE. **b.** SDS-PAGE of HsTFE from fractions of the IMAC and SEC steps of purification. **c, d.** BN-PAGE of anEcTFE purified in the presence of DDM, $C_{12}E_9$, LDAO, β-OG and CYMAL-6 detergent. M, BSA and MtTFE identify lanes with marker proteins, identifying molecular masses of (1236 kDa, 1048 kDa, 720 kDa, 480 kDa, 242 kDa, 146 kDa, 66 kDa and 20 kDa), (133 kDa and 66 kDa) and (240 kDa), respectively. **e.** BN-PAGE of HsTFE purified in the presence of $C_{12}E_9$, LDAO, DDM, CYMAL-6 and β-OG detergent.

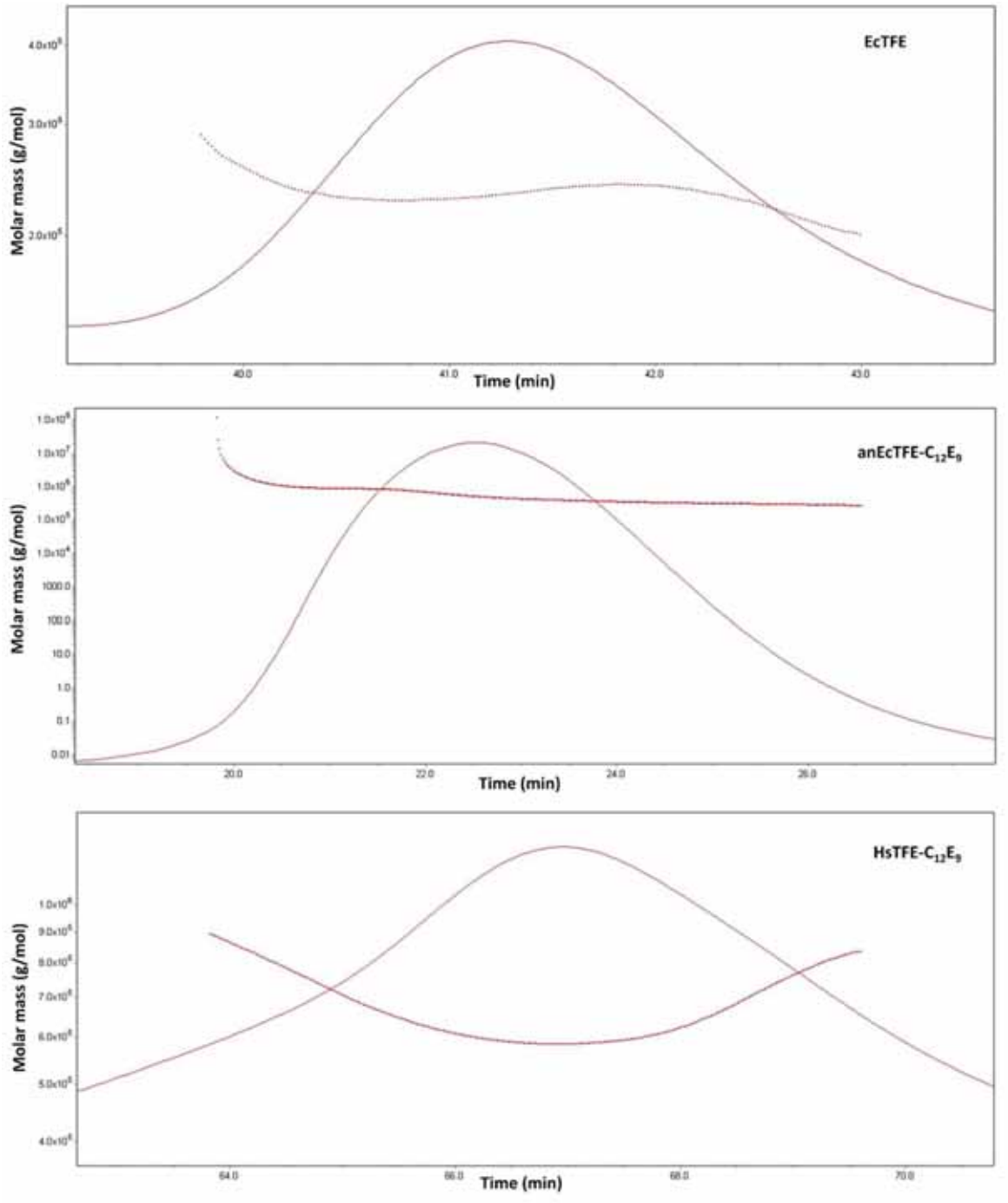

Supplementary Figure 4. The SEC-SLS analysis of EcTFE, anEcTFE (solubilized with $C_{12}E_9$ detergent) and HsTFE (solubilized with $C_{12}E_9$ detergent) using the Äkta Purifier equipped with a Superdex 200 10/300GL column (GE Healthcare), a Shodex refractive index detector and a Wyatt miniDAWN TREOS SLS detector. The plot of molar mass (horizontal red line) *versus* elution time is shown. Also shown is the corresponding SLS signal (curved red profile) showing the peaks of EcTFE, anEcTFE and HsTFE, eluting with an elution volume of 12.2 ml, 11.1 ml, and 10.9 ml respectively. The molecular mass of eluted EcTFE, anEcTFE and HsTFE is about 233 kDa, 535 kDa and 580 kDa respectively as calculated by the ASTRA Software.